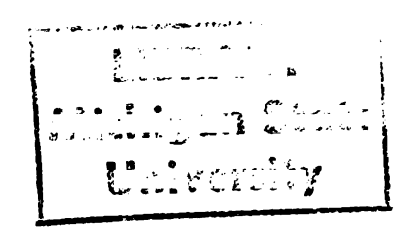
THS



This is to certify that the

dissertation entitled

A Numerical Method for the Treatment of Kinked Cracks in Finite Bodies

presented by

Ukhwan Sur

has been accepted towards fulfillment of the requirements for

Ph. D. degree in Mechanics

Date $\frac{2}{16/8}$

0-12771



RETURNING MATERIALS:

Place in book drop to remove this checkout from your record. FINES will be charged if book is returned after the date stamped below.

A NUMERICAL METHOD FOR THE TREATMENT OF KINKED CRACKS IN FINITE BODIES

Ву

Ukhwan Sur

A DISSERTATION

Submitted to

Michigan State University

in partial fullfillment of the requirements

for the degree of

DOCTOR OF PHILOSOPHY

Department of Metallurgy, Mechanics, and Materials Science

ABSTRACT

A NUMERICAL METHOD FOR THE TREATMENT OF KINKED CRACKS IN FINITE BODIES

Ву

Ukhwan Sur

A displacement discontinuity method is developed for modelling cracks in linear-elastic two-dimensional infinite domains. This method is then coupled to the standard boundary-element method for the treatment of cracks in finite two-dimensional regions. The hybrid approach has been implemented on the computer and representative results are presented. Problems studied include a variety of crack shapes, including cracks with kinks.

The hybrid method is shown to be an effective technique for the study of cracks of arbitrary shape in finite bodies. The ability of the method to handle cracks with kinks is a distinct advantage over other known approaches. Furthermore, the application of this method to crack propagation problems possesses none of the computational problems associated with other approaches.

ACKNOWLEDGEMENTS

I would like to express appreciation to those who have helped and contributed to making this work a reality. This includes my advisor, Dr. Nicholas J. Altiero, for his support, inspiration and assistance through this period and Drs. John F. Martin, Larry J. Segerlind and David Yen, members of my guidance committee. A final note of appreciation must go to my wife, Oksoon, for her tolerance and encouragement.

TABLE OF CONTENTS

			PAGE
LIST OF	TABI	LES	. iv
LIST OF	FIGU	JRES	v
CHAPTER	1	INTRODUCTION AND BACKGROUND	1
CHAPTER	2	BOUNDARY ELEMENT FORMULATION	8
		2.1 THE BOUNDARY INTEGRAL EQUATION METHOD	8
		2.2 NUMERICAL TREATMENT	12
CHAPTER	3	CRACK PROBLEMS: INFINITE DOMAIN	24
		3.1 THE DISPLACEMENT DISCONTINUITY METHOD	24
		3.2 NUMERICAL TREATMENT	30
CHAPTER	4	CRACK PROBLEMS: FINITE DOMAIN	35
		4.1 COUPLING OF BOUNDARY ELEMENT METHOD AND	
		DISPLACEMENT DISCONTINUITY METHOD	35
CHAPTER	5	EXAMPLES AND DISCUSSION	40
		5.1 EXAMPLES OF INFINITE DOMAIN CRACK PROBLEMS	40
		5.1.1 STRAIGHT CRACK	40
		5.1.2 CIRCULAR ARC CRACK	46
		5.1.3 KINKED CRACK	49
		5.2 EXAMPLES OF FINITE DOMAIN PROBLEMS	57
		5.2.1 STRAIGHT CRACK	57
		5.2.2 KINKED CRACK	66
CHAPTER	6	CONCLUSIONS AND RECOMMENDATIONS	71
RTRLTOGI	RAPHY	Ÿ	73

LIST OF TABLES

TABL	Æ	Page
2.1	Singular integrals	. 19
5.1	Displacement discontinuity along left half of a straight	
	crack in an infinite domain	. 44
5.2	Stress intensity factors at tip A of a kinked crack	
	$(\alpha_1 - 45^{\circ})$. 50
5.3	Stress intensity factors for an off-center straight crack	. 62
5.4	Stress intensity factors for an angled crack in a large plate	. 62
5.5	Stress intensity factors for an angled crack in a finite	
	plate	. 65

LIST OF FIGURES

FIGU	RE	Page
1.1	Crack propagation in an arbitrarily shaped body	. 7
2.1	Description of region of interest	. 9
2.2	Discretized model of region R	.13
2.3	Definition of vectors a and b	.17
3.1	Source point and field point in an infinite plane	.24
3.2	Line defining a crack in the infinite plane	.26
3.3	Equal and opposite crack surface tractions	. 29
3.4	Descretized crack surface	30
4.1	Center cracked plate with tensile load	36
4.2	Linear superposition of the boundary element and dispacement	
	discontinuity models	37
5.1	Straight crack in an infinite domain	40
5.2	Dependence of c on number of nodes	41
5.3	Dependence of c_n on location of transition node	43
5.4	Dependence of c_{n} on number of nodes when transition nodes	
	are used	.45
5.5	Circular arc crack	.46
5.6	SIFs for a circular arc crack under biaxial stress	.47
5.7	SIFs for a circular arc crack under pure shear	.48
5.8	Geometry of a kinked crack in an infinite plane	.49
5.9	Mode I SIFs for an asymmetric kinked crack under uniaxial	
		5 2

FIGURE

5.10	Mode II SIFs for an asymmetric kinked crack under uniaxial
	stress54
5.11	SIFs for an asymmetric kinked crack under various biaxial
	conditions55
5.12	SIFs for an anti-symmetric kinked crack in an infinite plate56
5.13	Center-cracked test specimen58
5.14	SIFs vs. a/b for center-cracked test specimen59
5.15	An off-center straight crack60
5.16	Angled crack in a large plate61
5.17	Angled crack in a finite plate64
5.18	Asymmetric kinked crack in a finite plate67
5.19	Anti-symmetric kinked crack in a finite plate68
5.20	SIFs for an asymmetric kinked crack in a finite plate69
5.21	SIFs for an anti-symmetric kinked crack in a finite plate70

INTRODUCTION AND BACKGROUND

The presence of cracks in a structure as shown in Figure 1.1 generally reduces the fatigue and static strength of the structure because the stresses and strains are highly magnified at the crack tip. It has been established that parameters deduced from linear elastic fracture mechanics can be used to determine the stress and strain magnification at the crack tip. These parameters, the stress intensity factors (SIF), incorporate applied load levels, geometry, and crack size in a systematic manner and may be evaluated from elastic stress analysis using the finite element method (FEM) or the boundary element method (BEM). The BEM is the numerical form of the "boundary integral equation method" (BIEM).

The FEM has been used extensively to solve elastic plastic problems in fracture mechanics. The FEM is very effective for solving problems with material and geometric nonlinearities, dynamic effects and inhomogeneities (e.g. boundaries, inclusions, interfaces). However, FEM is not the most effective method for problems involving singularities (e.g. mathematically sharp cracks) or localized events such as point sources and sinks. For the analysis of a sharp crack, a fine field discretization is needed near the crack tip to capture the rapidly varying stress and displacement fields. Furthermore, analysis of crack propagation necessitates constant re-defining of the finite element topology which may present severe computational difficulties.

The main disadvantage of the FEM is that a domain discretization is required to perform the analysis. The BEM involves discretization only of the boundary of the structure and the governing differential equation is solved exactly in the interior, leading to greater accuracy.

The boundary integral equation method has also been developed and extensively used for the analysis of problems in continuum mechanics. This method reduces the order of the problem, basically by using the divergence theorem of Gauss. However, the system matrix is full and unsymmetric so the reduction in order may be achieved only superficially. It is particularly effective for problems with singularities and dominantly linear response, and for modeling infinite domains. The method has also proven effective for the treatment of material nonlinearities. Geometric nonlinearities are still under study.

Several strategies have been proposed for the analysis of crack problems using the boundary integral equation method. These methods include representing the crack as a notch, symmetric crack modelling, use of special Green's functions, and flat crack modelling. Representing the crack as a notch or replacing the crack plane with symmetric boundary conditions, i.e. symmetric crack modelling, removes the singularity in the algebraic system of equations which is obtained when the upper and lower crack surfaces are modelled in the same plane [1]. However, representation of the crack as a notch increases the modelling error due to the notch opening and symmetric modelling is limited to symmetric problems. The special Green's function approach [2-4,5] possesses the advantage that crack geometry and crack tip

singularities are fully embedded in the boundary equations, i.e. no modelling of the crack surface is required. The disadvantage is that some two-dimensional and all three-dimentional problems can not be formulated using the special Green's function approach [4]. Also, complex arithmetic is required for the problems for which it does apply.

Flat crack modelling represents the displacements along the crack surface as the relative displacement between the two crack surfaces. This scheme has two critical deficiencies as a mathematical model for crack geometries, as pointed out by Cruse [4]. First, if there are no tractions on the outer boundary and only crack surface loading, a non-unique boundary integral equation is generated. Second, two unknown displacement variables, i.e. the relative and total displacements, exist along the crack. A possible solution for these problems is also given by Cruse [4]. An extensive discussion of the special Green's function and flat crack modelling techniques is given by Cruse [4]. The success of the BIEM in linear elasticity has motivated many attempts at application of this method to bodies containing cracks. These efforts have been hampered by certain difficulties associated with treating the two crack surfaces as "boundary" leading to an underdetermined system of equations.

In addition to BIEM, an alternative approach, suggested in [6,7,8], involves combining the boundary-integral equations of the two crack surfaces into a set of equations associated with a single surface integral. These new integral equations are precisely those obtained if one models the crack as a continuous layer of edge dislocations. The fact that a crack is equivalent to a continuous array of edge

dislocations has long been known [9]. Gol'dstein and co-workers employed this fact to develop an integral equation model for curvilinear cracks in an infinite plane subjected to arbitrary load. This method has since been developed for treatment of in-plane cracks of arbitrary shape. However, efforts to apply this technique to kinked cracks have not been successful [34].

The more important purpose of this work is to consider the behavior and characteristics of non-linear shaped cracks which are kinked, a phenomenon generally observed in the macroscopic or microscopic crack growth or propagation process.

Crack morphology seems to have significant meaning in crack propagation and fatigue crack growth. The brittle crack propagation and fatigue crack growth in the mixed mode loading state has received considerable attention. Generally in these cases a crack does not follow a straight path, but rather a curved or a kinked path.

Only a few reliable solutions for the stress intensity factors (SIF) of non-linear shaped cracks have been obtained for special cases. Some solutions for the stress intensity factors of non-linear shaped cracks in the state of longitudinal shear were given by Sih [10], Nakagama [11], and Smith et al. [12]. However analytic solutions for the stress intensity factors of non-linear shaped cracks in two-dimensional stress states which are more important to crack morphology are difficult to come by. Generally in these cases, both the stress intensity factors of mode 1 and mode 2 appear. For this reason, the analysis is not easy and many interesting problems can be expected to be found.

In this work we restrict our discussion to the problem of linear and non-linear shaped cracks in the two-dimensional elastic stress state. Recently, several experimental or numerical analyses for these kinds of problems have been reported [13]. Anderson [14] solves these problems on the basis of Muskhelishvili's method, but the value of his numerical results are questionable [15,16]. Kitagawa [17] constructed a general analytical method for determination stress intensity factors of non-linear shaped cracks in an infinite isotropic homogeneous plate in the two-dimensional elastic stress state. This method includes a polynomial approximation and truncation procedure [18] of a conformal mapping function. Also Kitagawa [17] obtained numerical results for various cases.

When a crack is oriented asymmetrically, the new crack initiates at an angle to the old one. The calculation of stress intensity factors for kinked cracks is difficult and there have been many attempts at their solution [19,20,21-24,25-28]. With most solutions, the analysis is such that the limit for an infinitesimally small kink cannot be obtained readily from the analysis for a finite kink. Recently, Lo [24] has presented a convincing solution that models the crack as a continuous distribution of dislocations, in a manner that can handle both the finite and the infinitesimal kink within the same formulation.

A new model, suggested here, has very good features in comparison with the edge dislocation model. This new set of integral equations is precisely that obtained if one models the crack as a line of displacement discontinuity. Knowledge of the edge dislocation distribution leads directly to the relative crack surface displacements

and to a complete field solution since the edge dislocation distribution is simply the derivative of the displacement discontinuity along the crack surface. It is, however, more appealing to formulate the equations in terms of the displacement discontinuity itself since the dislocation distribution is singular at tips but the displacement discontinuity is zero. The equations derived on this basis are, however, not integrable, a fact which has discouraged progress in this direction. An effort to develop a displacement discontinuity formulation has been presented by Crouch [29] but his numerical treatment results in modelling the crack as a discrete set of dislocation dipoles, a rather cumbersome variation of the dislocation density approach. Here, the displacement discontinuity is obtained through a single formulation and this method can handle kinked cracks very well. The displacement discontinuity method presented here is based on the analytical solution to the problem of a discontinuity in displacement over a finite line segment in an infinite elastic solid. Physically, one may imagine a displacement discontinuity as a line crack whose opposing surfaces have been displaced relative to one another. This method is based on the notion that one can make a discrete approximation to a continuous displacement discontinuity along a crack.

An effective hybrid method has also been developed here to model fracture problems in finite plane domains. This hybridization by (incrementally) linear superposition combines the best features of two component methods. Boundary elements are used to model the finite domain while a continuous distribution of displacement discontinuity (dislocation dipoles in two dimensions) are used to model the crack.

This method allows modelling of the crack "independently" of the Boundary Element mesh.

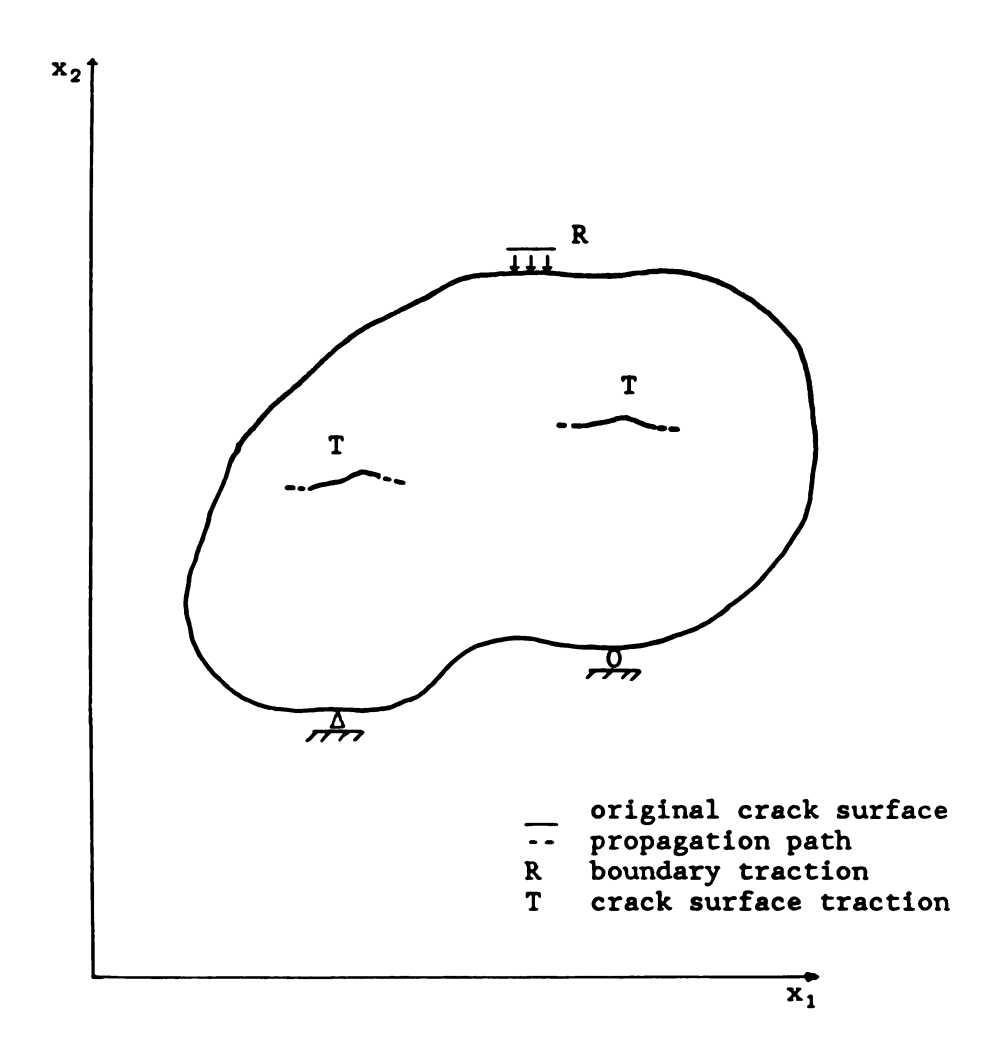


Figure 1.1. Crack propagation in an arbitrarily shaped body.

CHAPTER 2

BOUNDARY ELEMENT FORMULATION

2.1 THE BOUNDARY INTEGRAL EQUATION METHOD

For the plane boundary-value problem of linear elasticity illustrated in Figure 2.1, the displacement at a point x on B is related to the displacements and tractions at all other points on B by Somigliana's identity, i.e.

$$\alpha_{ij}(x)u_{j}(x) + \int_{B}(uc)_{i,j}(x,\bar{x})u_{j}(\bar{x})ds(\bar{x}) - \int_{B}(uR)_{i,j}(x,\bar{x})t_{j}(\bar{x})ds(\bar{x})$$
 (2.1)

where the integral on the left hand side is interpreted in the Cauchy principal-value sense. The function $(uc)_{i,j}(x,\bar{x})$ is the displacement in the i direction at x due to a unit displacement discontinuity applied in the j direction at \bar{x} in the infinite elastic plane and $(uR)_{i,j}(x,\bar{x})$ is the displacement in the i direction at x due to a unit force applied in the j direction at \bar{x} in the infinite elastic plane. The coefficients, α_{ij} , depend on the character of the boundary at x (e.g. $\alpha_{ij} = 1/2 \delta_{ij}$ at a smooth boundary point). As shall be seen, knowledge of α_{ij} is not required.

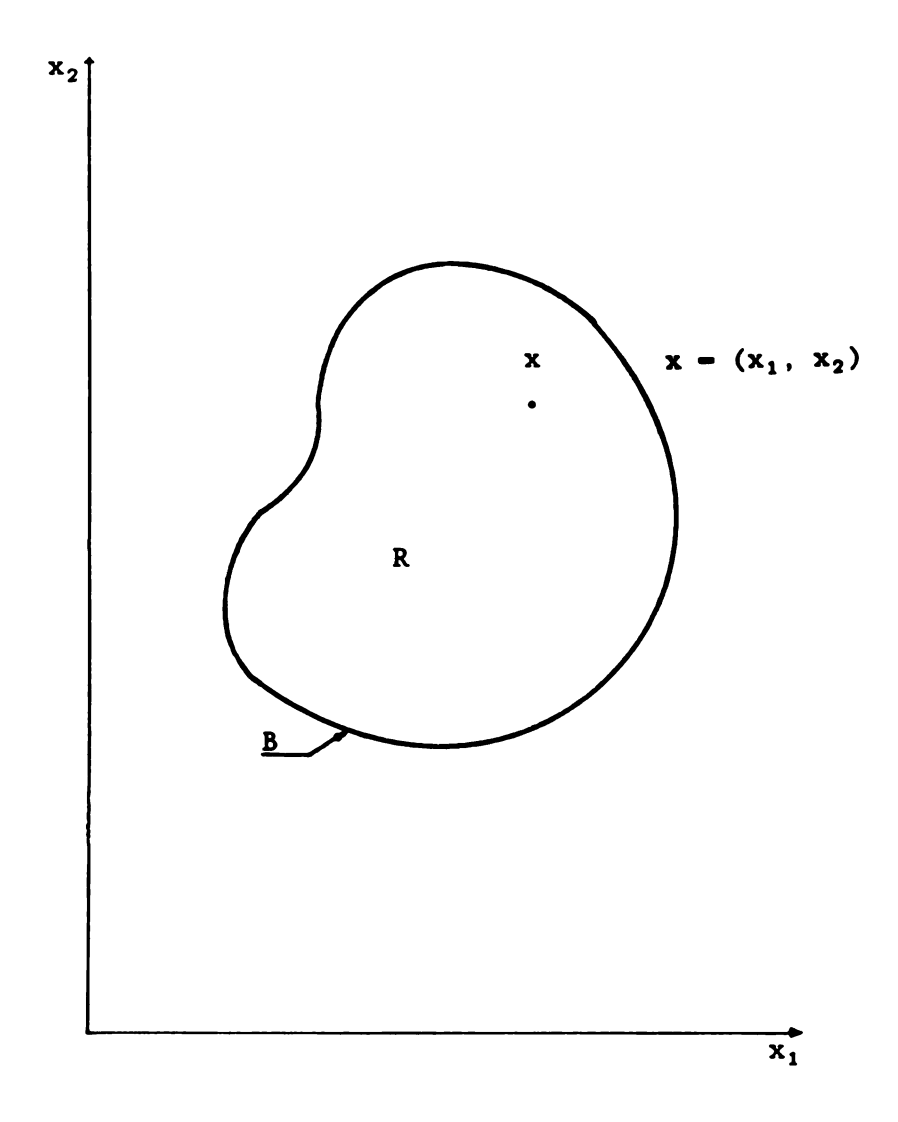


Figure 2.1 Description of region of interest.

At a point x in R, the displacements and stresses can be calculated from the equations

$$u_{i}(x) - \int_{B} (uR)_{i,j}(x,\bar{x}) t_{j}(\bar{x}) d\bar{s} - \int_{B} (uc)_{i,j}(x,\bar{x}) u_{j}(\bar{x}) d\bar{s}$$
 (2.2)

$$\sigma_{ik}(\mathbf{x}) = \int_{B}(\Pi R)_{ik.j}(\mathbf{x},\bar{\mathbf{x}}) t_{j}(\bar{\mathbf{x}}) d\bar{\mathbf{s}} - \int_{B}(\Pi c)_{ik.j}(\mathbf{x},\bar{\mathbf{x}}) u_{j}(\bar{\mathbf{x}}) d\bar{\mathbf{s}} \quad (2.3)$$

where the influence functions (ΠR)_{ik.j}(x,\bar{x}) and (Πc)_{ik.j}(x,\bar{x}) give the stress components at x due to a unit force applied in the j direction at \bar{x} , and a unit displacement discontinuity in the j direction at \bar{x} , respectively, in the infinite plane.

At each point x on B and in each direction, either $u_j(x)$ or $t_j(x)$ is known. Therefore, eq. (2.1) can be used to solve for the unknown values of $u_j(x)$ and $t_j(x)$, thus giving complete boundary information. The displacements and stresses at any internal point can then be determined by integration using eqs. (2.2) and (2.3).

It can be shown that, for plane stress, the influence functions of eqs. (2.1), (2.2) and (2.3) are given by

$$(uR)_{i,k} = [-(3-\nu)\delta_{ik}\log\rho + (1+\nu)q_iq_k]/(8\pi G)$$

$$(uc)_{1} = \frac{3}{1} - \frac{3$$

$$(uc)_{1_2} = [2(1+\nu)(-\bar{n}_2q_1 - \bar{n}_1q_2) + (1+3\nu)\bar{n}_2q_1 + (3+\nu)\bar{n}_1q_2]/(4\pi\rho)$$

$$(uc)_{2,1} = [2(1+\nu)(-\bar{n}_2q_1^3 - \bar{n}_1q_2^3) + (3+\nu)\bar{n}_2q_1 + (1+3\nu)\bar{n}_1q_2]/(4\pi\rho)$$

$$(uc)_{2,2} = [2(1+\nu)(-\bar{n}_1q_1+\bar{n}_2q_2) + (1-\nu)\bar{n}_2q_2 + (3+\nu)\bar{n}_1q_1]/(4\pi\rho)$$

$$(IIR)_{11} = [-2(1+\nu)q_1 - (1-\nu)q_1]/(4\pi\rho)$$

$$(IIR)_{12} = [2(1+\nu)q_2 - (3+\nu)q_2]/(4\pi\rho)$$

$$(IIR)_{22,1} = [2(1+\nu)q_1 - (1+3\nu)q_1]/(4\pi\rho)$$

$$(IIR)_{11}^{2} = [2(1+\nu)q_{2}^{3} - (1+3\nu)q_{2}]/(4\pi\rho)$$

$$(IIR)_{12_2} = [2(1+\nu)q_1^3 - (3+\nu)q_1]/(4\pi\rho)$$

$$(IIR)_{22} = [-2(1+\nu)q_2 - (1-\nu)q_2]/(4\pi\rho)$$

$$(\text{IIc})_{11_{-1}} = G(1+\nu) \left[(1+4q_1^2-8q_1^4) \bar{n}_1 + 2q_1q_2(1-4q_1^2) \bar{n}_2 \right] / (2\pi\rho^2)$$

$$(\text{IIc})_{12_1} = G(1+\nu)[(1-8q_1^2q_2^2)\bar{n}_2 + 2q_1q_2(1-4q_1^2)\bar{n}_1]/(2\pi\rho^2)$$

$$(\mathrm{IIc})_{22_{-1}} = \mathrm{G}(1+\nu)[(1-8q_1^2q_2^2)\bar{n}_1 + 2q_1q_2(1-4q_2^2)\bar{n}_2]/(2\pi\rho^2)$$

$$(\Pi c)_{11}_{2} - (\Pi c)_{12}_{1}$$

$$(IIc)_{12|2} - (IIc)_{22|1}$$

$$(\text{IIc})_{22_{2}} = G(1+\nu) \left[(1+4q_{2}^{2}-8q_{2}^{4})\bar{n}_{2} + 2q_{1}q_{2}(1-4q_{2}^{2})\bar{n}_{1} \right] / (2\pi\rho^{2})$$
(2.4)

where

$$\rho = [(x_1 - \bar{x}_1)^2 + (x_2 - \bar{x}_2)^2]^{1/2}$$

$$q_1 = (x_1 - \bar{x}_1)/\rho$$
 $q_2 = (x_2 - \bar{x}_2)/\rho$ (2.5)

and \bar{n}_1 , \bar{n}_2 are the components of the outward-directed unit normal vector at a point \bar{x} on the boundary, G is the shear modulus and ν is Poisson's ratio.

2.2 Numerical treatment

Eq. (2.1) can be solved numerically if the boundary B is approximated by N straight segments, as shown in Figure 2.2.

For this model, eq. (2.1) can be written as

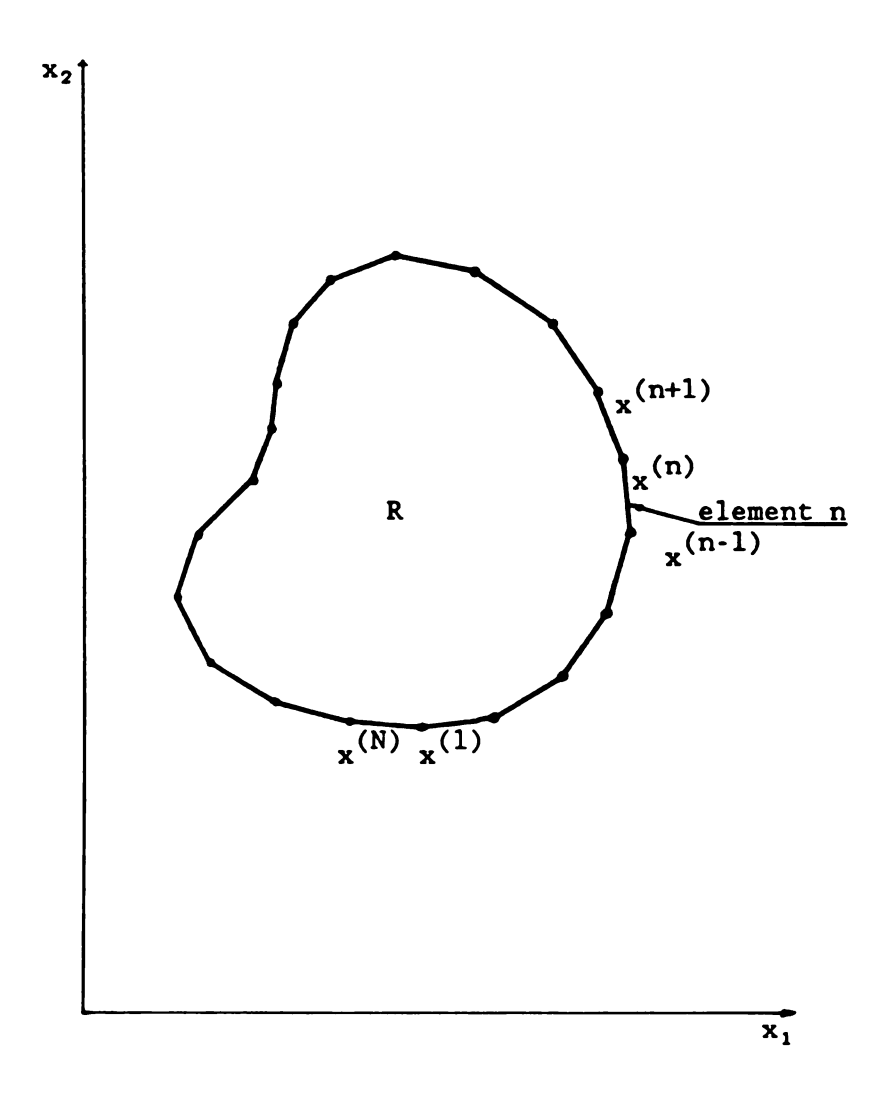


Figure 2.2 Discretized model of region R.

$$\alpha_{ij}^{(n)} u_{j}^{(n)} + \sum_{m=1}^{N} J_{m}^{(uc)} (uc)_{i,j}^{(n)} (x^{(n)}, \bar{x}) u_{j}^{(\bar{x})} d\bar{s}$$

$$-\sum_{m=1}^{N} \int_{m} (uR)_{i,j} (x^{(n)}, \bar{x}) t_{j}(\bar{x}) d\bar{s}$$
 (2.6)

where $u_j^{(n)}$ are the displacements components at node n and $n=1,\ldots,N,\ j=1,2.$

The displacements and tractions on each segment m can be approximated using shape functions so that

$$u_{j}(\bar{x}) - u_{j}^{(m-1)}N_{1}(\xi) + u_{j}^{(m)}N_{2}(\xi)$$

$$t_{j}(\bar{x}) - t_{j}^{(m)} \tag{2.7}$$

where

$$N_1(\xi) - (1-\xi)/2, N_2(\xi) - (1+\xi)/2$$

$$\bar{x} - N_1(\xi) x^{(m-1)} + N_2(\xi) x^{(m)}$$

$$d\bar{s} - [(s_m - s_{m-1})/2] d\xi - (\Delta s_m/2) d\xi \qquad (2.8)$$

and ξ is a local coordinate for the segment m with value -1 at node m-1, value 0 at the center of the segment, and value 1 at node m.

Note that the order of of $t_j(x)$ in the interval is less that that of $u_j(x)$. This model allows discontinuities of $t_j(x)$ on the boundary and it is consistent within elements, i.e. linear displacements and constant tractions on each element.

If eqs. (2.7) and (2.8) are substituted into eq. (2.6) the following is obtained

$$2 \hat{\alpha}_{ij}^{(n)} u_{j}^{(n)} + \Delta s_{m} \sum_{m=1}^{N} J_{m}(uc)_{i,j}(x^{(n)}, \xi)N_{1}(\xi)d\xi \cdot u_{j}^{(m-1)}$$

$$+ \Delta s_{m} \sum_{m=1}^{N} J_{m} (uc)_{i,j}(x^{(n)}, \xi)N_{2}(\xi)d\xi \cdot u_{j}^{(m)}$$

$$- \Delta s_{m} \sum_{m=1}^{N} J_{m}(uR)_{i,j}(x^{(n)}, \xi)d\xi \cdot t_{j}^{(m)}$$

or

$$2 \hat{\alpha}_{ij}^{(n)} u_{j}^{(n)} + \sum_{m=1}^{N} A_{i,j}^{(m,n)} u_{j}^{(m-1)} + \sum_{m=1}^{N} B_{i,j}^{(m,n)} u_{j}^{(m)}$$

$$- [1/G] \sum_{m=1}^{N} C_{i,j}^{(m,n)} \hat{F}_{j}^{(m)}$$

$$n=1, \dots, N$$
(2.9)

where

$$\hat{\alpha}_{ij}^{(n)} - \hat{\alpha}_{ij}^{(n)}$$

$$u_{j}^{(n)} - u_{j}(x^{(n)})$$

$$A_{i,j}^{(m,n)} - \Delta s_{m} J_{m}(uc)_{i,j}(x^{(n)},\xi)N_{1}(\xi)d\xi$$

$$B_{i,j}^{(m,n)} - \Delta s_{m} \int_{m} (uc)_{i,j} (x^{(n)}, \xi) N_{2}(\xi) d\xi$$

$$C_{i,j}^{(m,n)} - G \int_{m} (uR)_{i,j}(x^{(n)},\xi) d\xi$$

$$\hat{F}_{i,j}^{(m)} - \Delta s_m t_j^{(m)}$$
.

Note that two of the integrals on the left side of eq. (2.9) have been incorporated into the cofficients $\hat{\alpha}_{ij}^{(n)}$.

Now we must compute the following integrals for $m-1, \ldots, N$:

$$A_{i,j}^{(m,n)} - \Delta s_m \int_{-1}^{1} (uc)_{i,j} (x^{(n)}, \xi) N_1(\xi) d\xi$$
 m=n+1

$$B_{i,j}^{(m,n)} - \Delta s_m J_{-1}^{1}(uc)_{i,j}(x^{(n)},\xi)N_2(\xi)d\xi$$
 m=n (2.10)

$$C_{i,j}^{(m,n)} - G \int_{-1}^{1} (uR)_{i,j}(x^{(n)},\xi)d\xi$$

where (uc)_{i.j} and (uR)_{i.j} are given by eq. (2.4). To put (uc)_{i.j} and (uR)_{i.j} in the proper form, we require ρ , q_1 , q_2 , n_1 and n_2 as functions of ξ . Employing eq. (2.8), we have

$$x^{(n)} - \bar{x} = a_i - b_i \xi$$
 (2.11)

where we have defined

$$a_{i} - x_{i}^{(n)} - \hat{x}_{i}^{(m)}$$

and

$$b_i = x_i^{(m)} - \hat{x}_i^{(m)}$$

as shown in Figure 2.3.

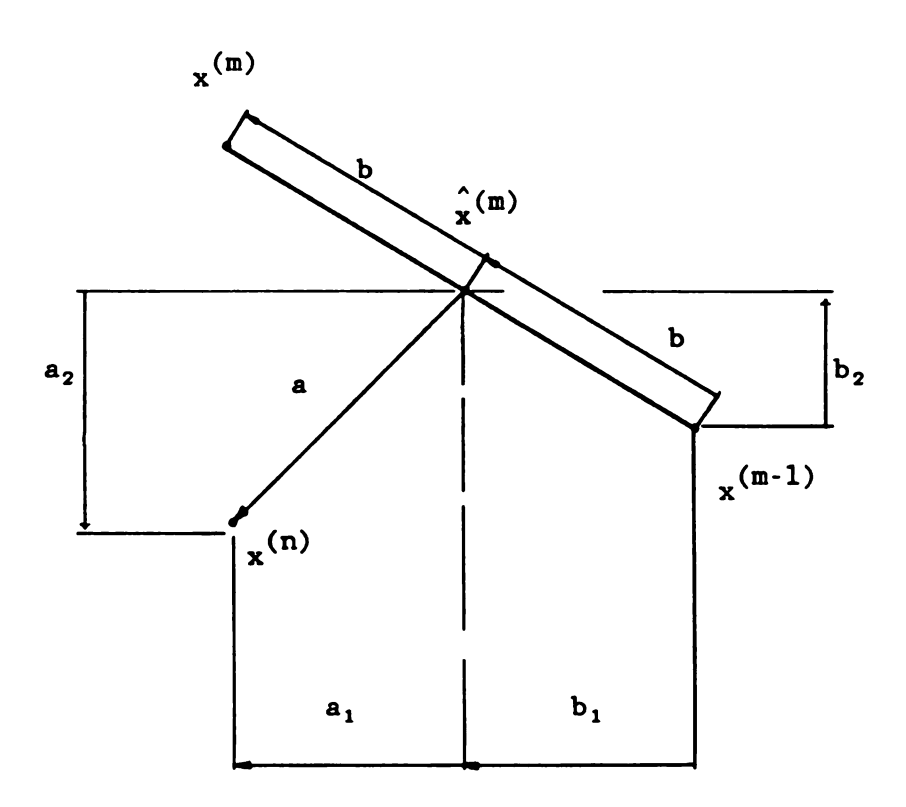


Figure 2.3 Definition of vectors ${\bf a}$ and ${\bf b}$.

Then

$$R = a_i a_i - 2a_i b_i \xi + b_i b_i \xi^2$$

$$q_1 - (a_1-b_1)/\rho$$
 $q_2 - (a_2-b_2)/\rho$ (2.12)

and

$$n_1 - (2/\Delta s_m) \cdot b_2$$
 $n_2 - (2/\Delta s_m) \cdot b_1$

The integrals given by eq. (2.10) can now be computed by Gaussian quadrature except for the following special integrals

$$A_{i,j}^{(m,n)} = \Delta s_{m} \int_{-1}^{1} (uc)_{i,j} (x^{(n)}, \xi) N_{1}(\xi) d\xi$$

$$C_{i,j}^{(m,n)} = G \int_{-1}^{1} (uR)_{i,j} (x^{(n)}, \xi) d\xi$$

$$B_{i,j}^{(m,n)} = \Delta s_{m} \int_{-1}^{1} (uc)_{i,j} (x^{(n)}, \xi) N_{2}(\xi) d\xi$$

$$C_{i,j}^{(m,n)} = G \int_{-1}^{1} (uR)_{i,j} (x^{(n)}, \xi) d\xi$$

$$m-n+1$$

A summary of those special integral calculations is shown in Table 2.1.

Table 2.1 Singular Integrals

n:node number m:segment number				
Condition	Coefficients	Value		
n-m-1,m	c (m.n) i.j	$[(3-\nu)(1-\log\Delta s_m)\delta_{ij}^{+(1+\nu)n_i^n_j}]/(4\pi)$		
n-m	$ \begin{bmatrix} A_{1,1}^{(m,n)} - A_{2,2}^{(m,n)} \\ B_{1,1}^{(m,n)} - B_{2,2}^{(m,n)} \end{bmatrix} $	0		
n-m-1	$B_{1,1}^{(m.n)} - B_{2,2}^{(m.n)}$			
n-m	$A_{1,2}^{(m.n)} = -A_{2,1}^{(m.n)}$	$(1- u)/(2\pi)$		
n-m-1	$B_{1,2}^{(m.n)} = -B_{2,1}^{(m.n)}$			

Eq. (2.9) can also be written in matrix form as

$$[uc](Gu) = [uR](\hat{F}).$$
 (2.14)

This is a system of equations relating nodal displacements to resultant segment forces. In order to solve a well-posed elasticity problem, it is necessary to re-pose this system of equations in terms of nodal forces. Therefore, a transformation

$$\{\mathbf{F}\} = [\Gamma](\hat{\mathbf{F}}) \tag{2.15}$$

relating the vector of nodal forces $\{F\}$ to the vector of segment forces $\hat{\{F\}}$, is introduced into the system (2.15). The simplest physical interpretation of the transformation is to replace the segment forces by nodal forces equal to the average of the segment forces adjacent to each node, or

$$F_i^{(n)} = 1/2 [\hat{F}_i^{(n)} + \hat{F}_i^{(n+1)}].$$
 (2.16)

The form of $[\Gamma]$ for this transformation is

$$[\Gamma] = 1/2$$

$$\begin{bmatrix}
1 & 1 & 0 & 0 & \cdot & \cdot & 0 \\
0 & 1 & 1 & 0 & \cdot & \cdot & 0 \\
0 & 0 & 0 & 1 & \cdot & \cdot & 0 \\
\cdot & \cdot & \cdot & \cdot & \cdot & \cdot & \cdot \\
\cdot & \cdot & \cdot & \cdot & \cdot & \cdot & \cdot \\
1 & 0 & 0 & 0 & . & . & 1
\end{bmatrix}$$

$$(2.17)$$

where I is a 2x2 identity matrix.

For an odd number of nodes, the inverse of $[\Gamma]$ is

$$[\Gamma]^{-1} = \begin{bmatrix} I & -I & I & -I & \cdot & \cdot & \cdot & I \\ I & I & -I & I & \cdot & \cdot & \cdot & -I \\ -I & I & I & -I & \cdot & \cdot & \cdot & I \\ I & -I & I & I & \cdot & \cdot & \cdot & -I \\ & \cdot \\ -I & I & -I & I & \cdot & \cdot & \cdot & I \end{bmatrix}$$
 (2.18)

and eq. (2.14) becomes

$$[uc](Gu) = [uR][\Gamma]^{-1}(F).$$
 (2.19)

It should be noted that, for an even number of nodes, $[\Gamma]$ has no inverse.

We can obtain the diagonal 2x2 blocks of [uc] through a simple observation. If we apply a rigid body displacement to the body (i.e. $u_1^1 - u_1^2 - \ldots - u_1^N$, $u_2^1 - u_2^2 - \ldots - u_2^N$), this will generate no stress so that $\{F\} = \{0\}$ and it follows that

$$(uc)_{(2n-1)(2n-1)} = \sum_{\substack{n=1 \\ m \neq n}}^{N} (uc)_{(2n-1)(2m-1)}$$

$$(uc)_{(2n-1)(2n)} = \sum_{\substack{n=1 \\ m \neq n}}^{N} (uc)_{(2n-1)(2m)}$$

$$(uc)_{(2n)(2n-1)} = \sum_{m=1}^{N} (uc)_{(2n)(2m-1)}$$

$$(uc)_{(2n)(2n)} = \frac{N}{m-1} (uc)_{(2n)(2m)}$$
 (2.20)

After solving eq. (2.19), stresses and displacements can be calculated anywhere in the body using a discretized form of eqs. (2.2) and (2.3), i.e.

$$u_{i}^{(n)} - \sum_{m=1}^{N} J_{m}(uc)_{i,j}(x^{(n)}, \bar{x}) u_{j}(\bar{x}) d\bar{s}$$

$$+ \sum_{m=1}^{N} J_{m}(uR)_{i,j}(x^{(n)}, \bar{x}) t_{j}(\bar{x}) d\bar{s} \qquad (2.21)$$

$$\sigma_{ik}^{(n)} = -\sum_{m=1}^{N} J_m(\Pi c)_{ik,j}(x^{(n)},\bar{x}) u_j(\bar{x}) d\bar{s}$$

$$+ \sum_{m=1}^{N} J_{m}(\Pi R)_{ik,j}(x^{(n)}, \bar{x}) t_{j}(\bar{x}) d\bar{s}$$
 (2.22)

where i=1,2, k=1,2, $u_i^{(n)}$ are the displacements at field point $x^{(n)}$, and $\sigma_{ik}^{(n)}$ are the stresses at $x^{(n)}$.

If eqs. (2.7) and (2.8) are substituted into eqs. (2.21) and (2.22) the following is obtained

$$u_{i}^{(n)} - \Delta s_{m} \sum_{m=1}^{N} J_{m}(uc)_{i,j}(x^{(n)}, \xi)N_{1}(\xi)d\xi \cdot u_{j}^{(m-1)}$$

$$- \Delta s_{m} \sum_{m=1}^{N} J_{m}(uc)_{i,j}(x^{(n)}, \xi)N_{2}(\xi)d\xi \cdot u_{j}^{(m)}$$

$$+ \Delta s_{m} \sum_{m=1}^{N} J_{m}(uR)_{i,j}(x^{(n)}, \xi)d\xi \cdot t_{j}^{(m)} \qquad (2.23)$$

$$\sigma_{ik}^{(n)} = -\Delta s_{m} \sum_{m=1}^{N} J_{m}^{(\Pi c)}_{ik.j}^{(x^{(n)},\xi)N_{1}(\xi)d\xi \cdot u_{j}^{(m-1)}}$$

$$-\Delta s_{m} \sum_{m=1}^{N} J_{m}^{(\Pi c)}_{ik.j}^{(x^{(n)},\xi)N_{2}(\xi)d\xi \cdot u_{j}^{(m)}}$$

$$+\Delta s_{m} \sum_{m=1}^{N} J_{m}^{(\Pi R)}_{ik.j}^{(x^{(n)},\xi)d\xi \cdot t_{j}^{(m)}}$$
(2.24)

Eqs. (2.23) and (2.24) can also be written in matrix form as

$$\begin{cases} u_1^{(n)}(x) \\ u_1^{(n)}(x) \end{cases} = [uR^*][\Gamma]^{-1} \{F\} - [uc^*]\{Gu\}$$
 (2.25)

$$\begin{cases}
\sigma_{11}^{(n)}(x) \\
\sigma_{22}^{(n)}(x) \\
\sigma_{12}^{(n)}(x)
\end{cases} = [IIR^{*}][\Gamma]^{-1} \{F\} - [IIc^{*}]\{Gu\} \tag{2.26}$$

All the entries of the matrices [uR*], [uc*], [Ic*] and [IIR*] are calculated by numerical integration using Gauss-Legendre quadrature (Conte and deBoor [36]).

CHAPTER 3

CRACK PROBLEMS: INFINITE DOMAIN

3.1 The Displacement Discontinuity Method

Consider an infinite elastic plane in which there is a point, \bar{x} , at which some "source" of stress is located and a field point, x, at which the stresses are to be computed. At each of these points, we will be referring to small integral surfaces as shown in Figure 3.1 described by unit normals \bar{n} , and n, respectively.

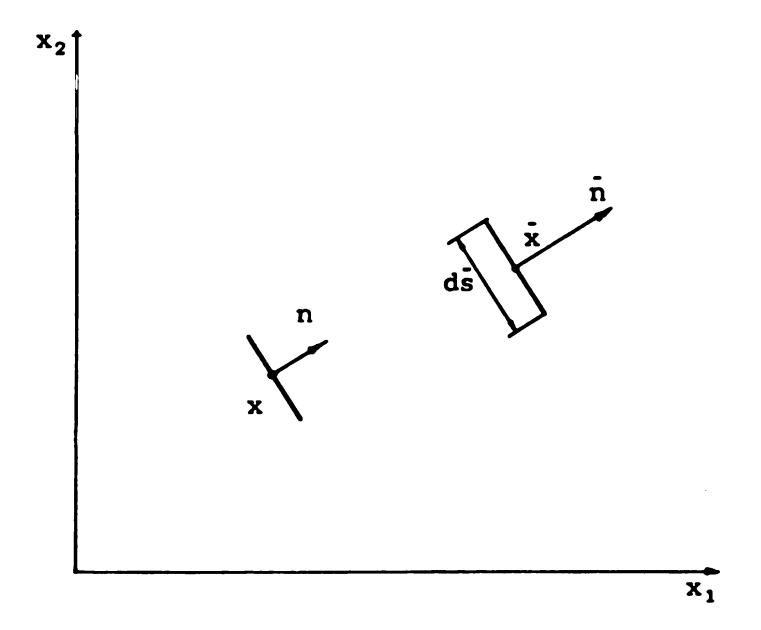


Figure 3.1 Source point and field point in an infinite plane.

Let us define functions π_1 and π_2 at x such that

$$\sigma_{11} = \frac{\partial \pi_1}{\partial \mathbf{x}_2} \qquad \qquad \sigma_{22} = \frac{\partial \pi_2}{\partial \mathbf{x}_1}$$

$$\sigma_{12} = -\frac{\partial \pi_1}{\partial \mathbf{x}_1} = \frac{\partial \pi_2}{\partial \mathbf{x}_2}.$$
(3.1)

If we now introduce displacement discontinuities of unit magnitude in the x_1 and x_2 directions at \bar{x} , we can obtain :

$$(\pi c)_{1,1} = \frac{G(1+\nu)}{2\pi\rho} [2\bar{n}_2 q_1^3 + 2\bar{n}_1 q_2^3 - \bar{n}_2 q_1 - 3\bar{n}_1 q_2]$$

$$(\pi c)_{1,2} = (\pi c)_{2,1} = \frac{G(1+\nu)}{2\pi\rho} [2\bar{n}_1 q_1^3 - 2\bar{n}_2 q_2^3 - \bar{n}_1 q_1 + \bar{n}_2 q_2]$$

$$(\pi c)_{2,2} = \frac{G(1+\nu)}{2\pi\rho} [-2\bar{n}_2 q_1^3 - 2\bar{n}_1 q_2^3 + 3\bar{n}_2 q_1 + \bar{n}_1 q_2]$$

$$(3.2)$$

where $(\pi c)_{1,1} = \pi_1$ at x due to a unit displacement discontinuity in the i direction, at \bar{x} in the infinite domain, etc.

Next consider a line of length ℓ , as shown in Figure 3.2, across which the displacement is discontinuous by amounts $c_1(s)$ and $c_2(s)$.

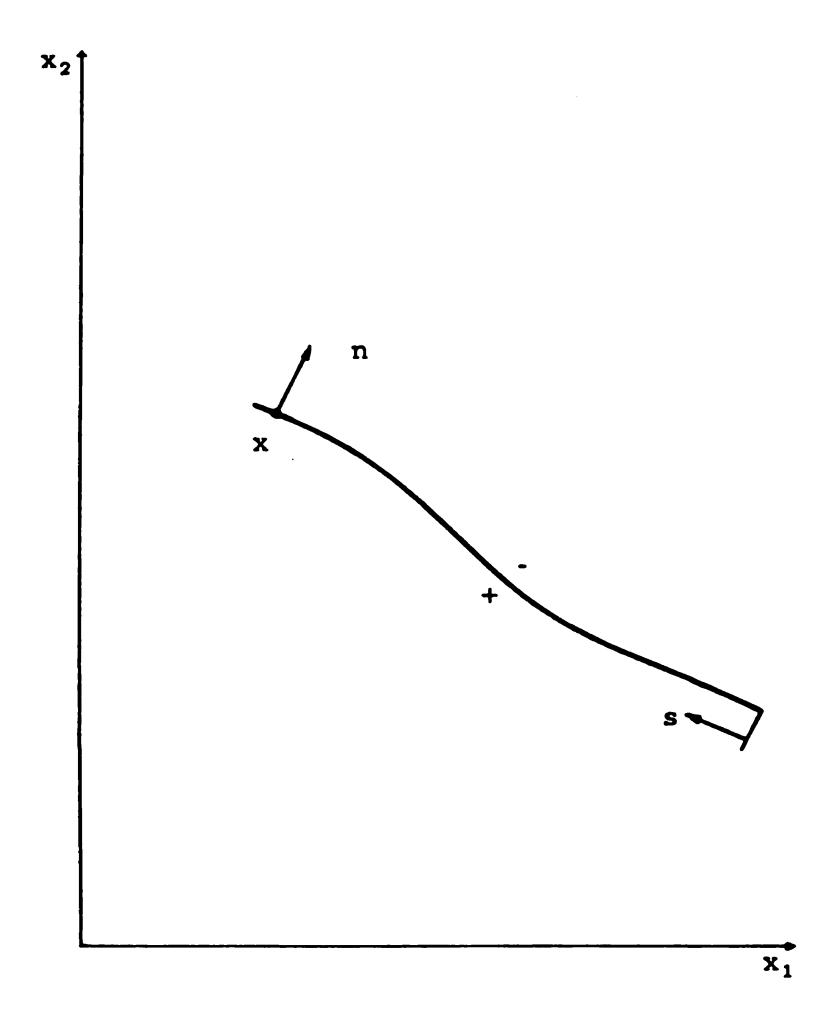


Figure 3.2 Line defining a crack in the infinite plane.

Then, by superposition, we have at x:

$$\pi_{1} = \int_{0}^{\ell} [(\pi c)_{1,1} c_{1} + (\pi c)_{1,2} c_{2}] d\bar{s}$$

$$\pi_{2} = \int_{0}^{\ell} [(\pi c)_{2,1} c_{1} + (\pi c)_{2,2} c_{2}] d\bar{s}$$
(3.3)

where $c_i - u_i^-$, i-1,2, and all integrals are interpreted in the Cauchy principal-value sense.

Suppose that the line is a crack, the surfaces of which are subjected to equal and opposite tractions $t_1(s)$ and $t_2(s)$ as shown in Figure 3.3. Then,

$$t_{1}^{*} = -\left[\sigma_{11}n_{1} + \sigma_{12}n_{2}\right]$$

$$= -\left[\frac{\partial \pi_{1}}{\partial x_{2}} \frac{dx_{2}}{ds} + \frac{\partial \pi_{1}}{\partial x_{1}} \frac{dx_{1}}{ds}\right]$$

$$= -\frac{d\pi_{1}}{ds}$$
(3.4)

and similarly

$$t_2^* - - \frac{d\pi_2}{ds} \tag{3.5}$$

so that

along the crack, and eqs.(3.3) become

$$\int_{0}^{\ell} [(\pi c)_{1}]_{1} c_{1} + (\pi c)_{1}]_{2} c_{2} d\bar{s} - J_{s_{0}}^{s} t_{1}^{*} d\bar{s}$$

$$\int_{0}^{\ell} [(\pi c)_{1}]_{2} c_{1} + (\pi c)_{2}]_{2} c_{2} d\bar{s} - J_{s_{0}}^{s} t_{2}^{*} d\bar{s}.$$
(3.7)

Thus, if $t_1^*(s)$ and $t_2^*(s)$ are given, eqs.(3.7) can be solved for $c_1(s)$ and $c_2(s)$. Then the displacement discontinuities normal and tangential to the crack surfaces are

$$c_n - c_1 n_1 + c_2 n_2$$

$$c_t - c_2 n_1 - c_1 n_2.$$
(3.8)

Once $\mathbf{c}_{\mathbf{n}}$ and $\mathbf{c}_{\mathbf{t}}$ are known, we can readily compute the stress intensity factors as follows

$$K_{I}|_{s=0} - \frac{E}{8} \int \frac{2\pi}{\epsilon} c_{n}(\epsilon)$$

$$K_{II}|_{s=0} - \frac{E}{8} \int \frac{2\pi}{\epsilon} c_{t}(\epsilon)$$

$$K_{I}|_{s=\ell} - \frac{E}{8} \int \frac{2\pi}{\epsilon} c_{n}(\ell - \epsilon)$$
(3.9)

where $\epsilon << \ell$.

 $K_{II}|_{s=\ell} - \frac{E}{8} / \frac{2\pi}{\epsilon} c_t(\ell - \epsilon)$

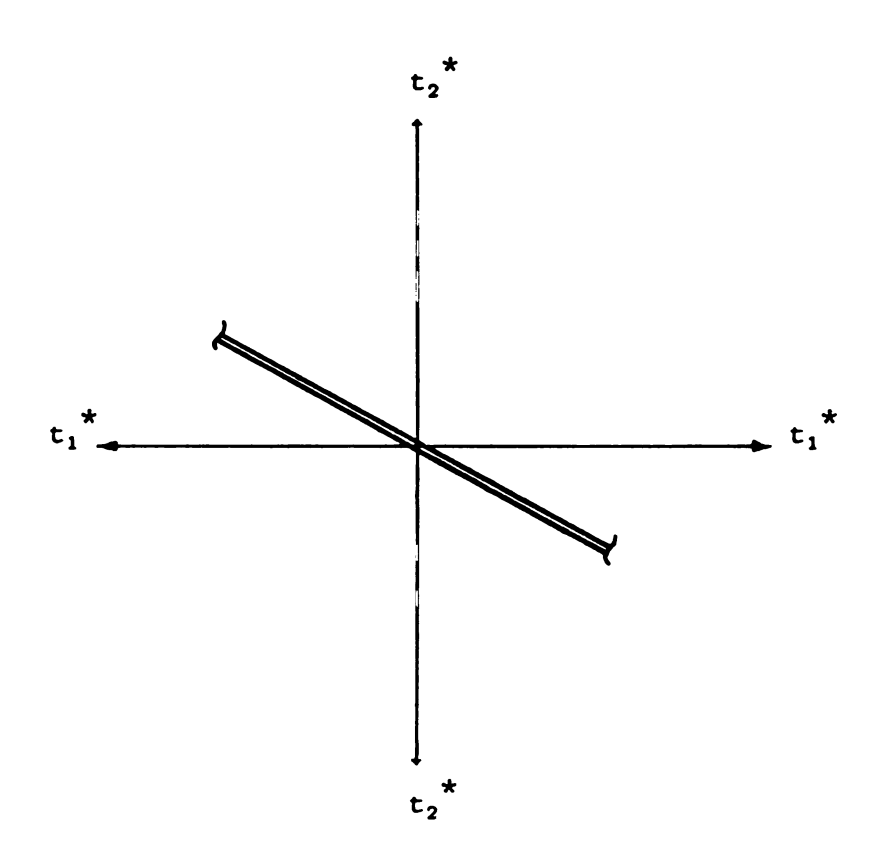


Figure 3.3 Equal and opposite crack surface tractions.

3.2 Numerical Treatment

Eq. (3.7) can be solved numerically if the crack surface is approximated by N straight segments, as shown in Figure 3.4

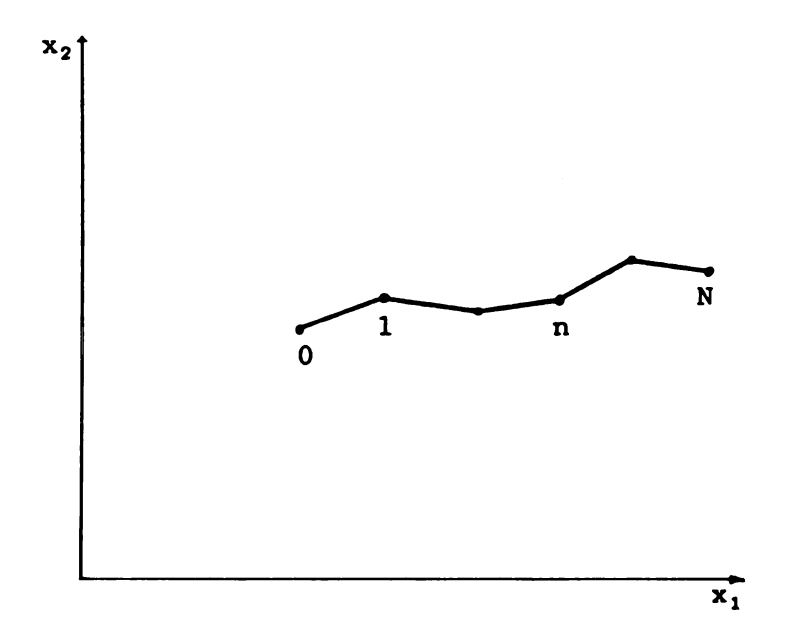


Figure 3.4 Discretized crack surface.

For this model, eq. (3.7) can be written as

$$\sum_{m=1}^{N} \int_{m} (\pi c)_{i,j} (x^{(n)}, \bar{x}) c_{j} (\bar{x}) d\bar{s} = -\pi_{i}^{*(n)}$$
(3.10)

where $x^{(n)}$ is the mid-point of element n, n = 1,..,N, and summation on j is implied.

The displacement discontinuities in each segment m can be approximated using shape functions so that

$$c_{j}(\bar{x}) = N_{1}c_{j}^{(m-1)} + N_{2}c_{j}^{(m)}$$
 (3.11)

where

$$N_1(\xi) = (1-\xi)/2, N_2(\xi) = (1+\xi)/2$$

$$-1 \le \xi \le 1$$

$$\bar{x} = N_1(\xi) x^{(m-1)} + N_2(\xi) x^{(m)}$$
(3.12)

$$d\bar{s} = [(s_m - s_{m-1})/2] \cdot d\xi = [\Delta s_m/2] \cdot d\xi.$$

If eq. (3.11) and (3.12) are substituted into eq. (3.10) the following is obtained

$$G_{m-1}^{N}[A_{i,j}^{(m,n)}c_{j}^{(m-1)} + B_{i,j}^{(m,n)}c_{j}^{(m)}] = -\pi_{i}^{*(n)}$$
(3.13)

where

$$A_{i,j}^{(m,n)} - J_m N_1 D_{i,j}^{(m,n)} d\xi$$

$$B_{i,j}^{(m,n)} - J_m N_2 D_{i,j}^{(m,n)} d\xi$$

$$D_{i,j}^{(m,n)} = [(s_m - s_{m-1})/(2G)] \cdot (\pi c)_{i,j} (x^{(n)}, \xi).$$

It is noted that $c_1^{(0)} - c_2^{(0)} - c_1^{(N)} - c_2^{(N)} - 0$.

Note that the function (πc) is singular when the integration variable ξ approaches the mid point of node n. This is the case when the element m is a neighbor of the node n. The resulting singular integrals must be handled analytically. The singular integrals for i - j reduce to

$$D_{1,1}^{(m,n)} - D_{2,2}^{(m,n)} - \frac{(1+\nu)}{4\pi\xi}$$

and the integrals involving $i \neq j$ are zero. Thus,

$$A_{i,j}^{(m,n)} = B_{i,j}^{(m,n)} = 0$$
 $i \neq j$ (3.14)

whereas, for i-j

$$A_{1,1}^{(m,n)} - A_{2,2}^{(m,n)} - \frac{(1+\nu)}{2\pi}$$

$$B_{1,1}^{(m,n)} - B_{2,2}^{(m,n)} - \frac{(1+\nu)}{2\pi}. \tag{3.15}$$

If eqs. (3.14) and (3.15) are substituted into eq. (3.13), the following equations are obtained

$$-\frac{G(1+\nu)}{2\pi} c_{1}^{(n-1)} + \frac{G(1+\nu)}{2\pi} c_{1}^{(n)}$$

$$+G \sum_{m=1}^{N} [A_{1}^{(m,n)} c_{j}^{(m-1)} + B_{1}^{(m,n)} c_{j}^{(m)}] = -\pi_{1}^{*(n)}$$
(3.16)

and

$$-\frac{G(1+\nu)}{2\pi} c_{2}^{(n-1)} + \frac{G(1+\nu)}{2\pi} c_{2}^{(n)}$$

$$+G_{\substack{m=1\\m\neq n}}^{N} [A_{2}^{(m,n)} c_{j}^{(m-1)} + B_{2}^{(m,n)} c_{j}^{(m)}] - -\pi_{2}^{*(n)}$$
(3.17)

where n-1,...,N and $c_{j}^{(0)} - c_{j}^{(N)} - 0$.

In matrix form, we have

$$[\pi c] \{Gc\} = \{-\pi^*\}.$$
 (3.18)

Let the nodal force vector be given by

$$T_i^{(n)} = [-\pi^{*(n+1)} + \pi^{*(n)}]$$

or

$$\{T\} = [\Gamma_2] \{-\pi^*\}$$
 (3.19)

where

is 2(N-1)x2N. Then

$$[\Gamma_2][\pi c]\{Gc\} - \{T\}.$$
 (3.21)

This is the system of equations one needs to analyze a crack in the infinite plane subjected to crack surface tractions.

CHAPTER 4

CRACK PROBLEMS: FINITE DOMAIN

4.1 <u>Coupling of Boundary Element Method and Displacement Discontinuty</u> Model

Consider the problem (shown in Figure 4.1) of a center-cracked plate with a boundary load R and a crack surface load, T. This problem can be analysed using linear superposition, as shown in Figure 4.2. Linear superposition allows representation of the actual problem as a sum of a boundary element model and a crack model. The vector $\mathbf{R}_{\mathbf{C}}$ is the correction applied (only at the boundary) to the load vector R in the BEM to account for the presence of a crack. The vector $\mathbf{T}_{\mathbf{C}}$ is the correction applied (only along the crack surface) to the traction vector T in the crack model to account for the finite boundary of the actual problem. What is now required is force matching along the crack surface.

Using eq. (2.19), which was discussed in Chapter 2, the governing boundary element equations for the center-cracked plate are given by

$$[uc](u) = [uR][\Gamma]^{-1}(R-R_c).$$
 (4.1)

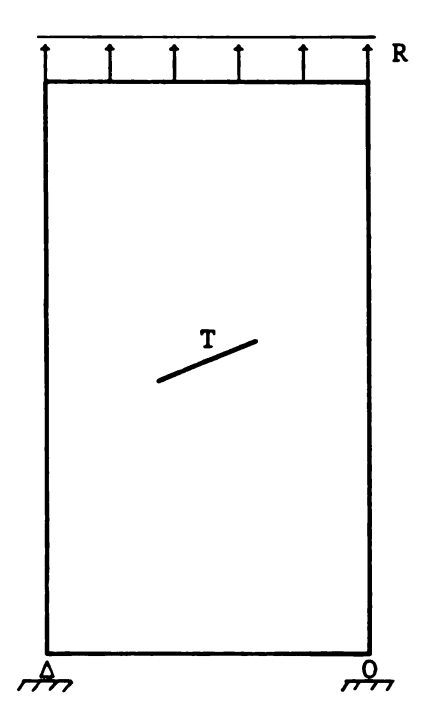


Figure 4.1. Center cracked plate with tensile load.

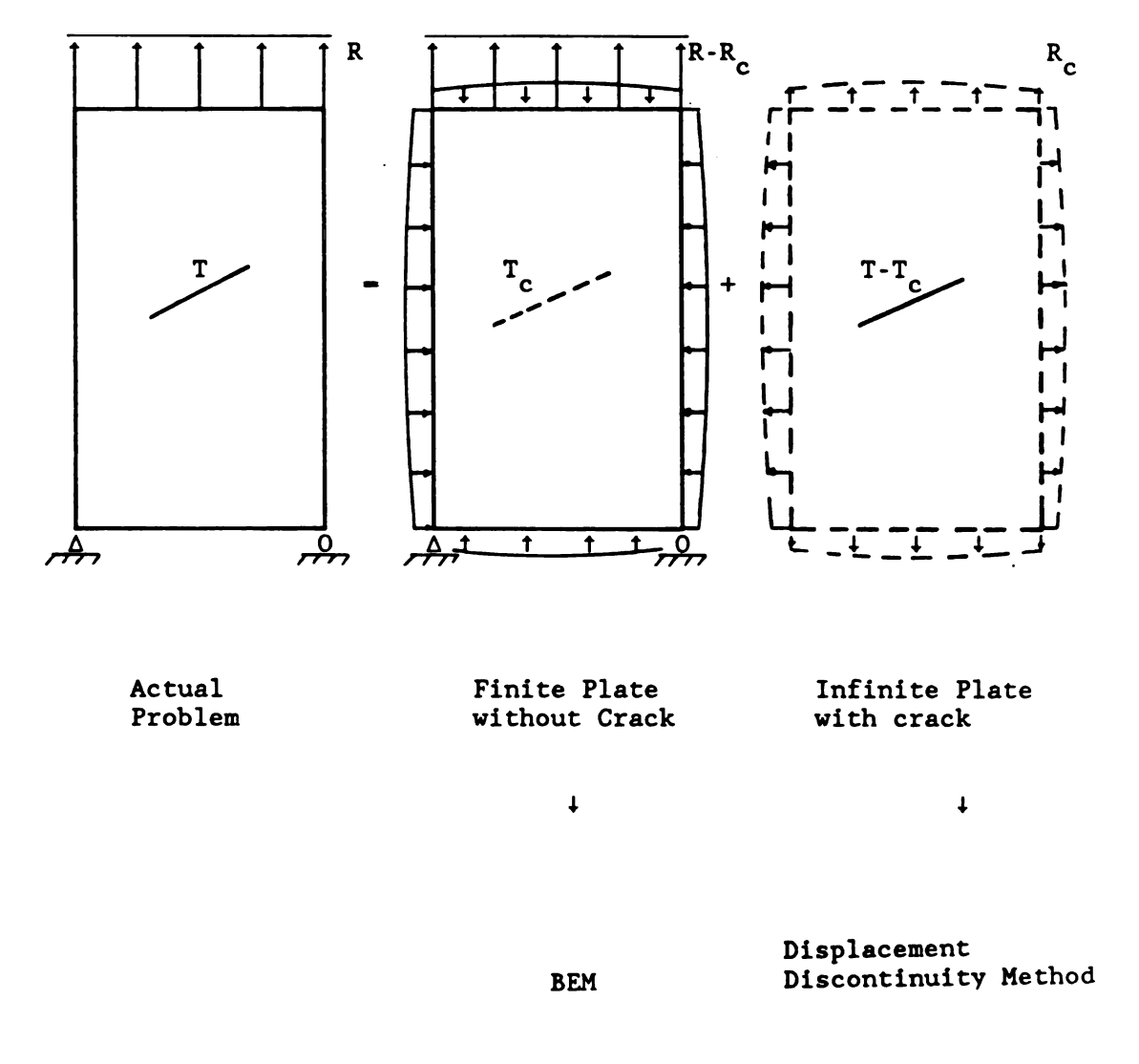


Figure 4.2 Linear superposition of the boundary element and displacement discontinuity models.

This is a system of equations relating nodal displacements to resultant nodal forces.

The load correction vector $\mathbf{R}_{\mathbf{C}}$ can be written as a function of the displacement discontinuity vector \mathbf{c} using matrix [$\Pi \mathbf{c}$]

$$\{R_{C}\} = [SN][IIc](Gc)$$

$$(4.2)$$

where [SN] is a normal matrix multiplied by the unit area. Combining equations (4.1) and (4.2), gives

$$[uc](Gu) + [uR][\Gamma]^{-1}[SN](\Pi c)(Gc) - [uR][\Gamma]^{-1}(R).$$
 (4.3)

The crack model is the result of modeling crack(s) in an infinite medium using a continuous distribution of displacement discontinuity. The discretized equations for the infinite plate with crack are given by

$$-[\Gamma_2][\pi c]\{Gc\} - \{T\} - \{T_c\}. \tag{4.4}$$

Using eq. (2.26) which was discussed in Chapter 2, the correction vector $\mathbf{T}_{\mathbf{C}}$ can be expressed as a function of the displacement vector \mathbf{u} using matrices [IIR] and [IIc]

$$\{T_c\} = [SN][\Pi R][\Gamma]^{-1} \{R - R_c\} - [SN][\Pi c]\{Gu\}.$$
 (4.5)

Combining eqs. (4.4) and (4.5), we have

$$\{T\} = [SN][\Pi R][\Gamma]^{-1}\{R-R_c\} - [SN][\Pi c]\{Gu\} - [\Gamma_2]\{[\pi c]\{Gc\}\}.$$
 (4.6)

To eliminate vector R_c , eq. (4.2) is substituted into eq. (4.6), so that

$$[SN][\Pi c](Gu) + \{[SN][\Pi R][\Gamma]^{-1}[SN][\Pi c] + [\pi c]\}(Gc)$$

$$= [SN][\Pi R][\Gamma]^{-1}(R) - \{T\}. \tag{4.7}$$

Equations (4.3) and (4.7) result in a coupled matrix system.

This is the system of equations needed to solve crack problems in finite plane domains.

In equation (4.9) it is noted that the vector u represents the continuous displacement field at the boundary element nodes, not the total displacement field in the actual problem. However, the vector c represents the displacement discontinuity only for the finite plate with crack so that the vector c for the finite plate without crack is always zero.

CHAPTER 5

EXAMPLES AND DISCUSSION

5.1 Examples of Infinite Domain Crack Problems

5.1.1 Straight crack

Here we employ the displacement discontinuity method to find a numerical approximation of the relative normal displacement between the two surfaces of a straight crack loaded uniaxially as shown in Figure 5.1. It can be shown that the solution to this problem is equivalent to that due to uniform pressure applied to the crack surfaces. Altiero [33] obtained the solution shown in Figure 5.2 by assuming linear variation of the displacement discontinuity on each element and computing integrals by using the trapezoidal rule.

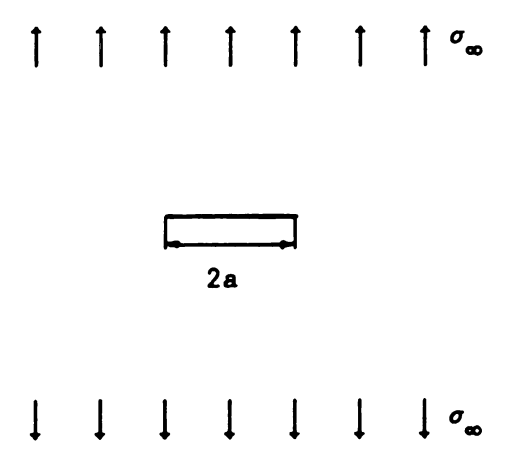
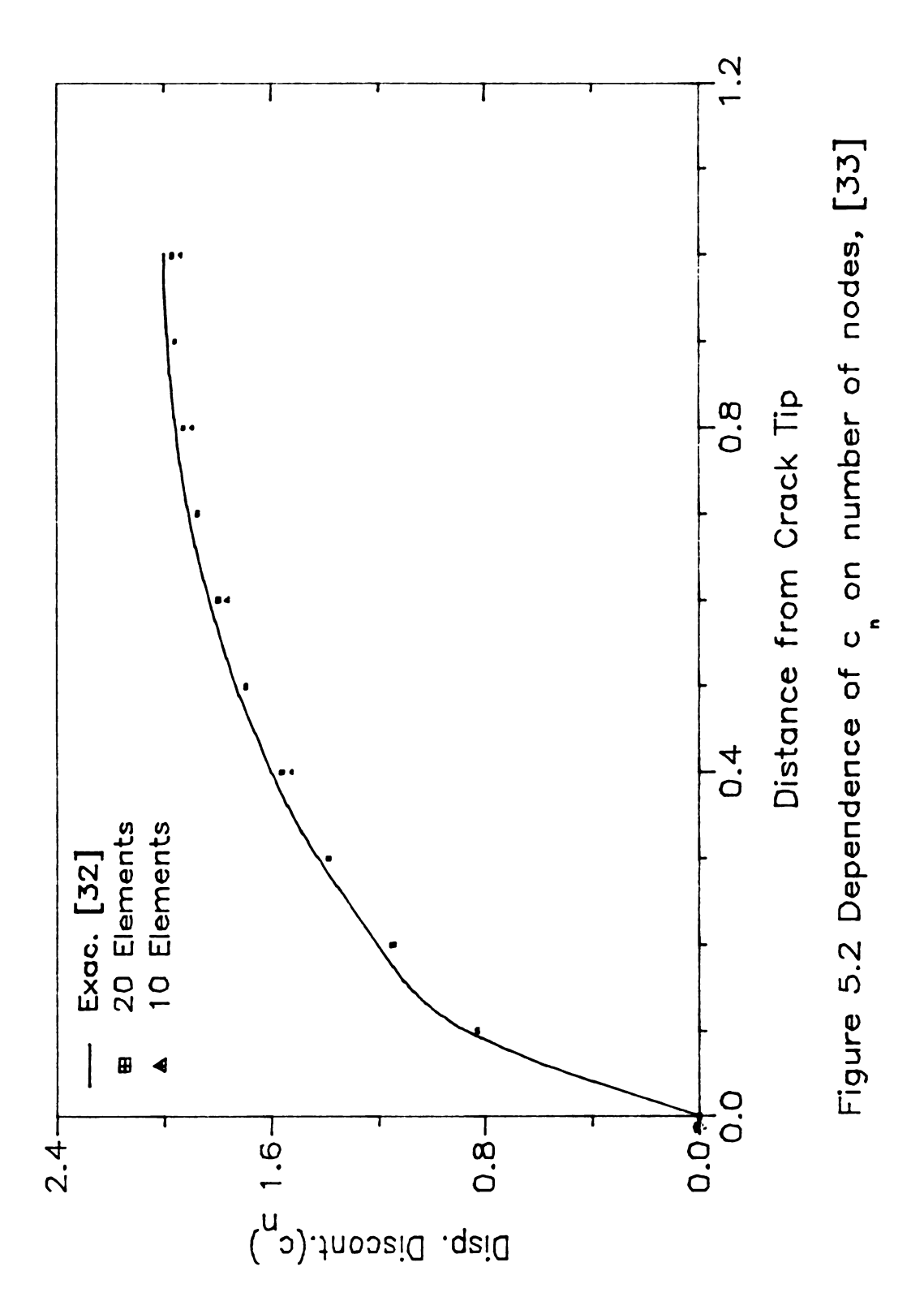
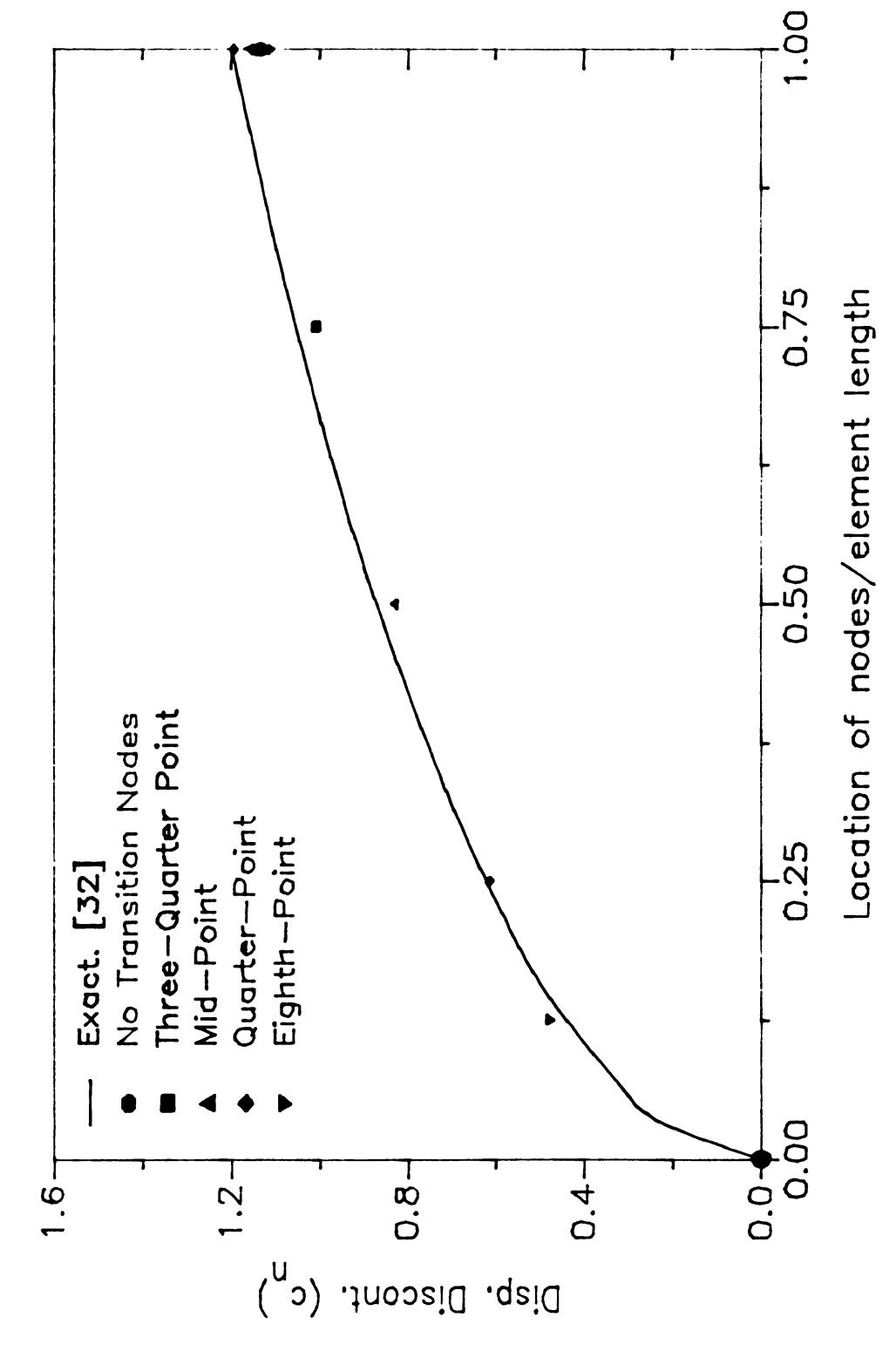


Figure 5.1 Straight crack in an infinite domain.



Since, in fracture mechanics problems, an accurate solution near the crack tip is important, a more sophisticated approach is needed. In this work the determination of crack tip stress intensity factors is carried out using equally-spaced nodes except for additional "transition" nodes near the crack tips. As an example, the pressurized crack problem is analysed using additional nodes located at one-quarter of the distance from the crack tip to the next adjacent node. The quarter-point location was selected based on a trial-and-error procedure. Figure 5.3 presents the comparison of the displacement discontinuities (c_n) for several cases of transition node locations. A significant improvement in accuracy using quarter-point transition nodes is evident. This remarkable improvement is not achieved by increasing the number of degrees-of-freedom but merely by shifting of the nodes nearest the crack-tips.

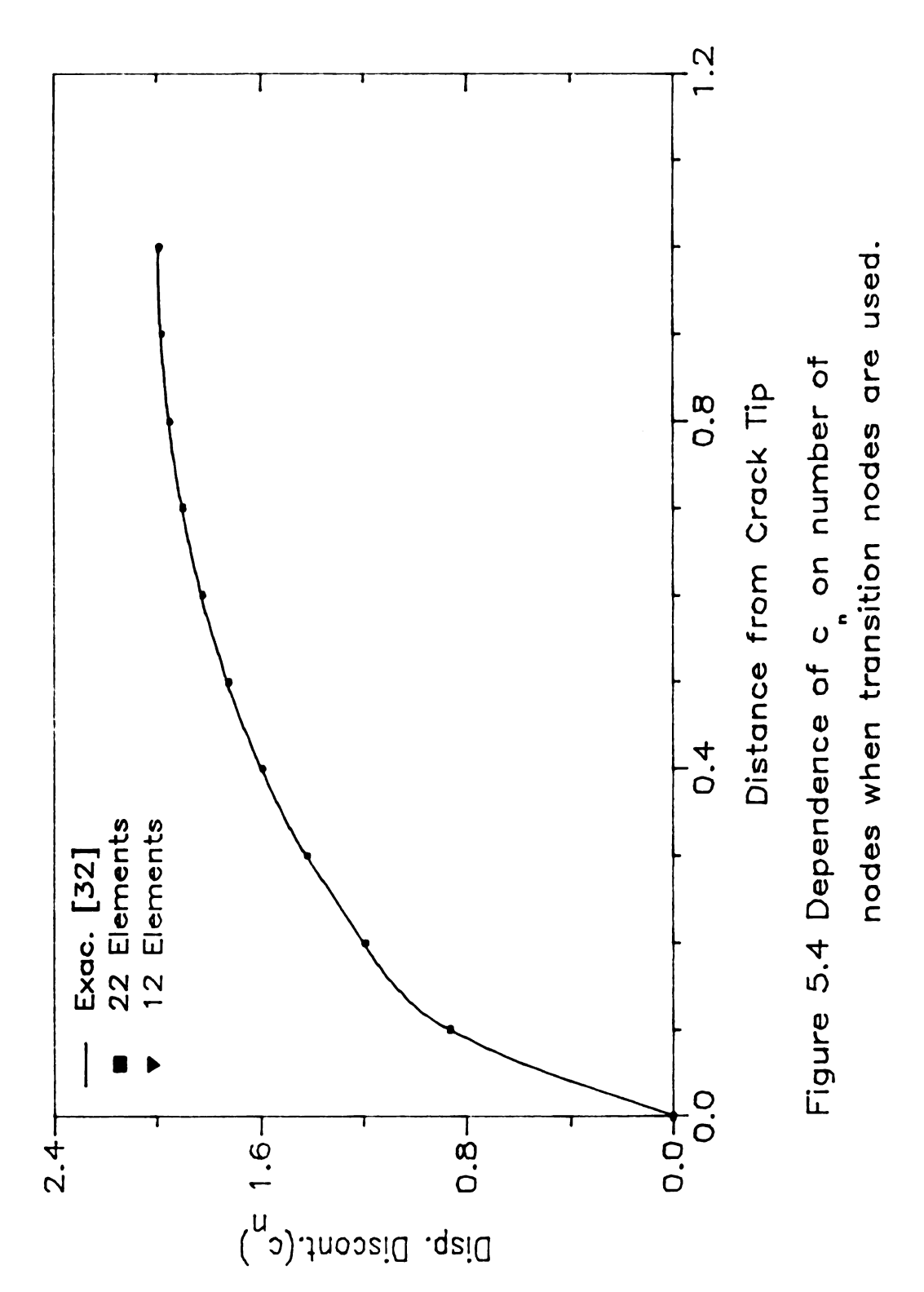
Two solutions to the problem of Figure 5.1, using quarter-point nodes are shown in Figure 5.4 and Table 5.1. These results are plotted in dimensionless form, valid for arbitrary values of crack length 2a and shear modulus G. The first approximation was found by dividing the length of the crack (2a) into 10 equal elements while the second was found by dividing it into 20 equal elements. In both cases two additional quarter-point nodes were added. Thus, the first approximation involved 12 elements and the second involved 22 elements. The discontinuities, c_n , are assumed linear over each element. It appears from Figure 5.4 that the displacement discontinuity method underestimates the relative displacements between the crack surfaces, but the results tend to the exact solution as N is increased. The solution is symmetric about x = 1.



Dependence of c_n on location of transition node. Figure 5.3

Table 5.1 Displacement discontinuty along left half of a straight crack in an infinite domain.

distance from crack tip	analytical solution[33]	numerical solution		[CRACK]
		(12 elements)	(22	elements)
0.025	0.4444	-		0.4373
0.050	0.6244	0.6150		•
0.100	0.8717	-		0.8660
0.200	1.2000	1.1926		1.1929
0.300	1.4282	-		1.4199
0.400	1.6000	1.5898		1.5916
0.500	1.7320	-		1.7239
0.600	1.8330	1.8213		1.8250
0.700	1.9078	-		1.9000
0.800	1.9595	1.9476		1.9518
0.900	1.9895	-		1.9823
1.000	2.0000	1.9880		1.9923



5.1.2 Circular arc crack

Because an exact solution exists, the circular arc crack subjected to uniform stress applied at infinity provides a simple check on the accuracy of the numerical solution. This problem is shown in Figure 5.5. The solution, given by Sih, Paris and Erdogan [30] was obtained using the method of Mushkelishvili [31]. The solution obtained by the present method and the exact solution are compared in Figures 5.6 and 5.7 for biaxial and shear stress loading at infinity. In both cases the numerical solution for the displacement discontinuity is accurate to within 2 %. The stress intensity factors are accurate to within 1 % everywhere.

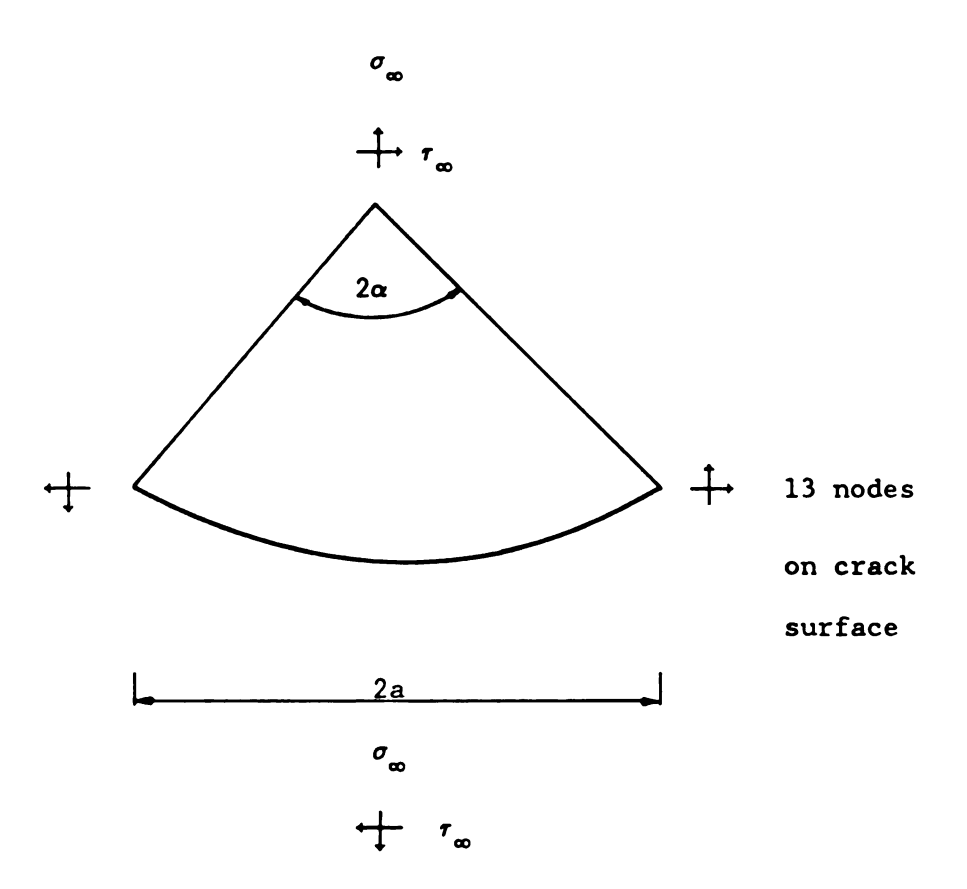
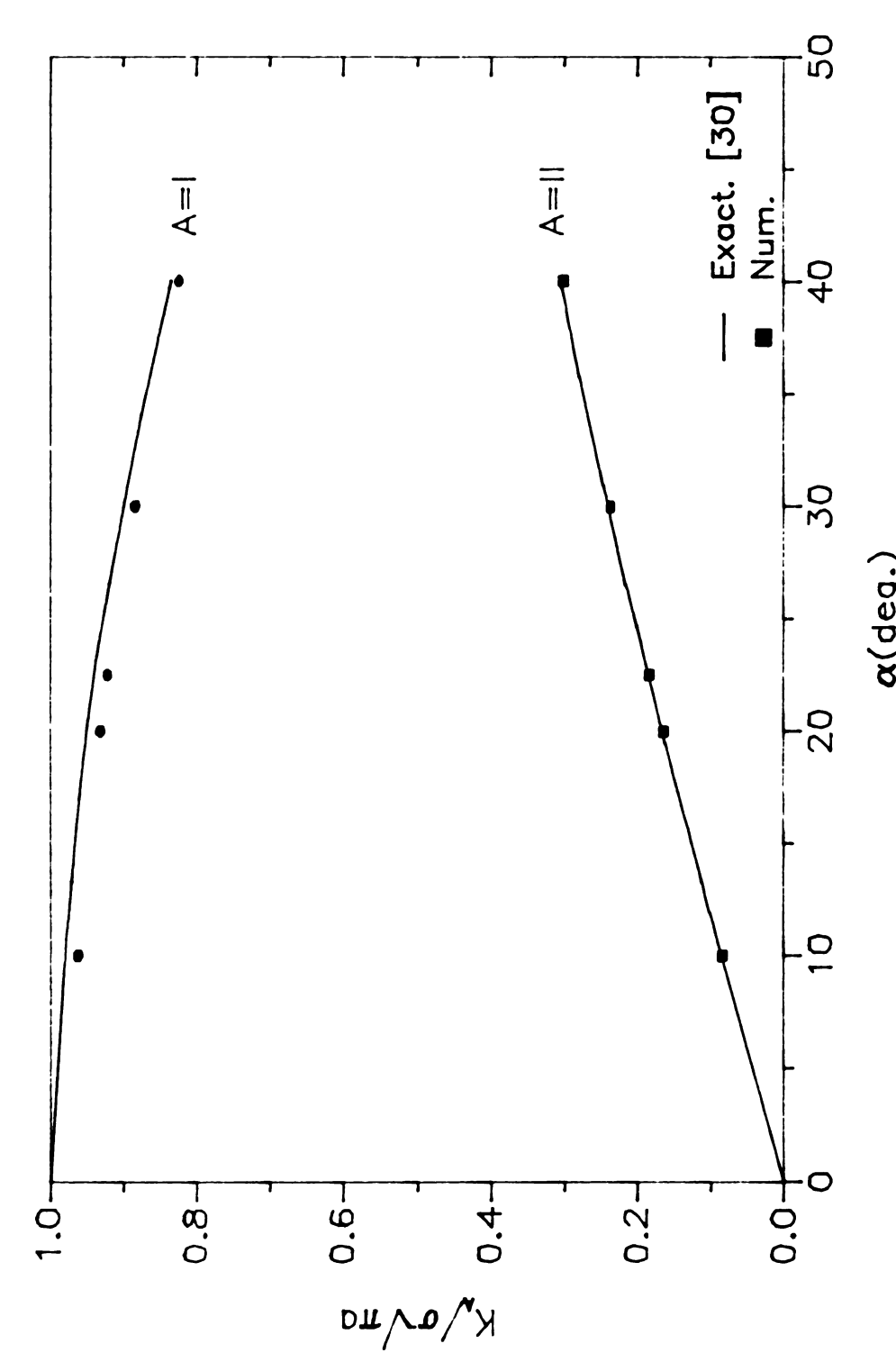
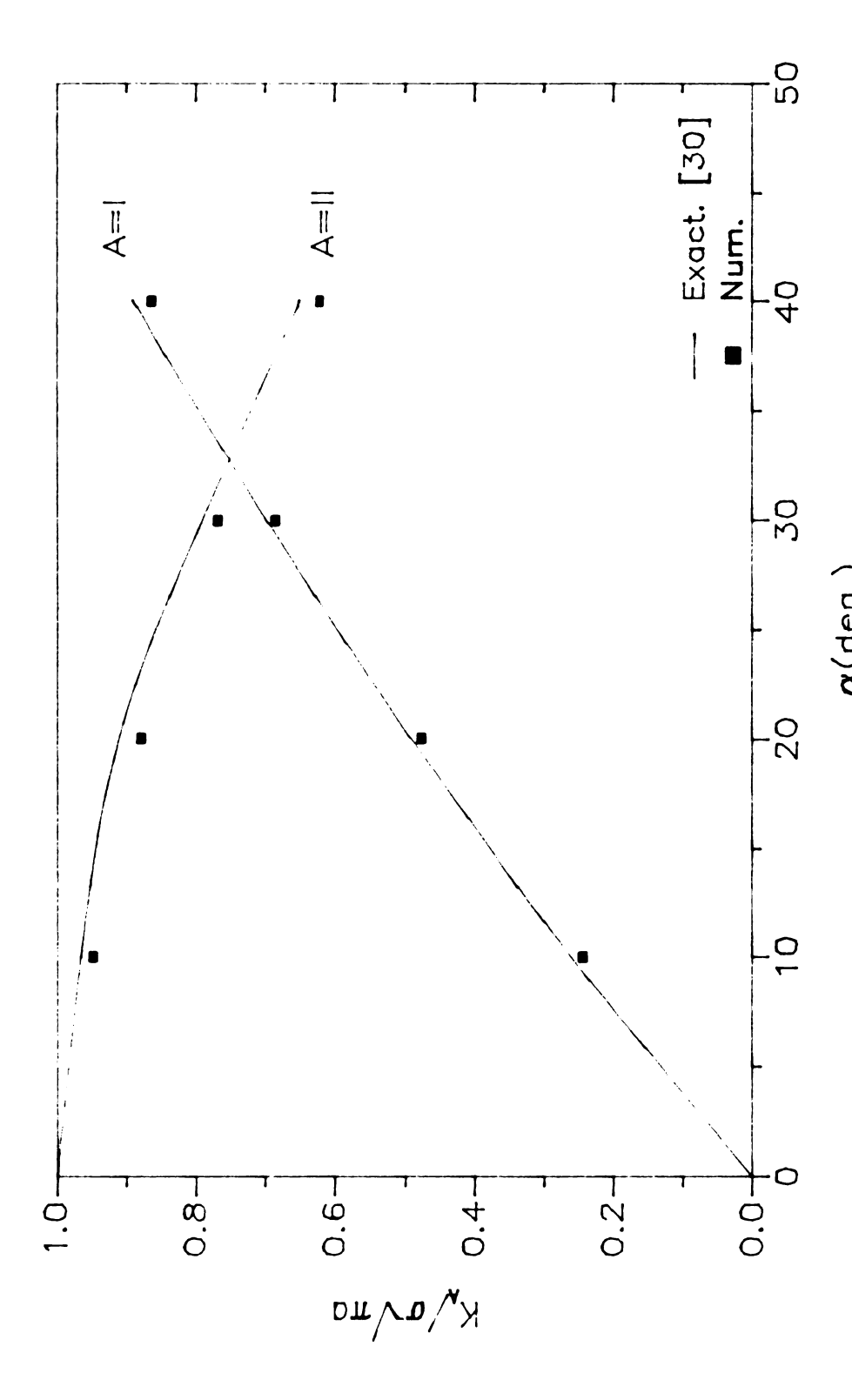


Figure 5.5 Circular arc crack.



 $lpha({
m deg.})$ Figure 5.6 SIFs for a circular arc crack under biaxial stress.



 $\alpha(\mbox{deg.})$ Figure 5.7 SIFs for a circular arc crack under pure shear.

5.1.3 Kinked crack

We next consider the basic kinked crack problem shown in Figure 5.8. The branches are sharp cracks of length b_1 and b_2 inclined to the plane of the original crack by angles α_1 and α_2 , respectively.

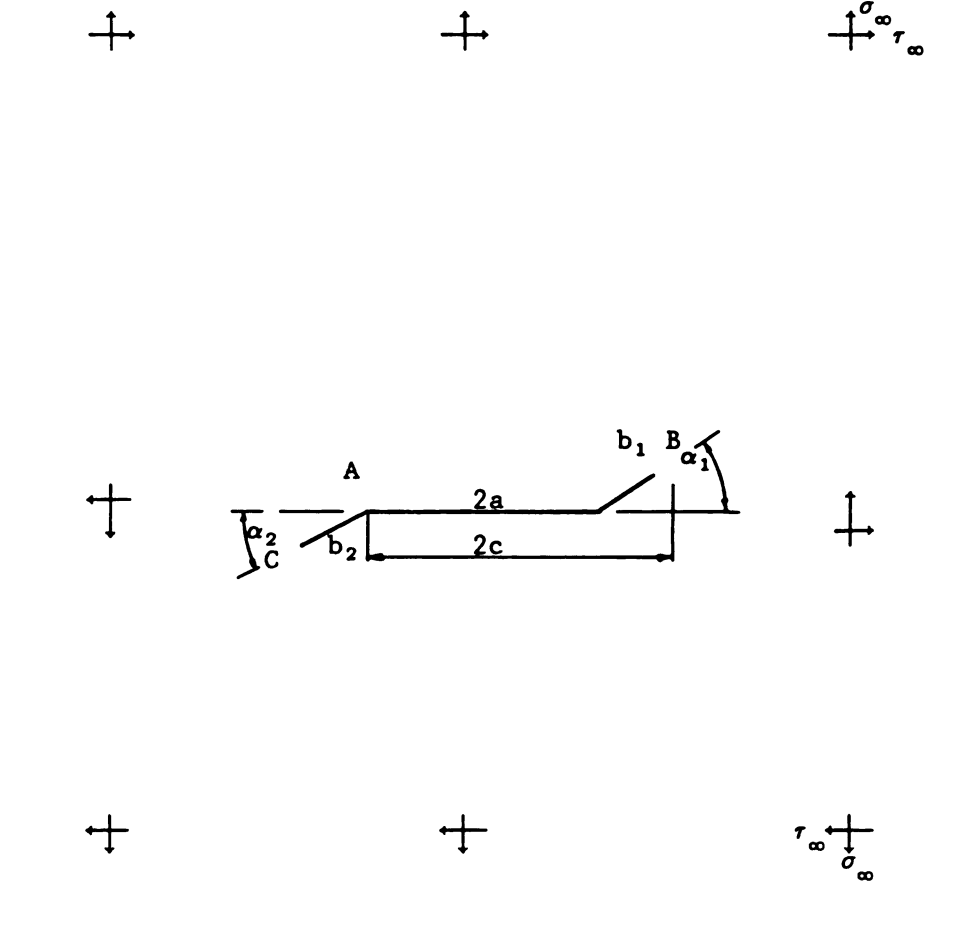


Figure 5.8 Geometry of a kinked crack in an infinite plane.

(a) Asymmetric kinked crack

First, we consider a crack with a right side branch only as shown in Figure 5.8, i.e. an "asymmetric kinked crack". the projected length, 2c, is defined by

$$2c = 2a + b_1 \cos \alpha_1$$
. (5.1)

The stress intensity factors at the crack tip A of the asymmetric kinked crack are shown in Table 5.2 for α_1 = 45 and two values of b_1 . These are normalized with respect to the stress intensity factors for a straight crack with the crack length 2c projected along the direction perpendicular to the tensile axis, i.e. $F_{1A} = \frac{K_I}{\sigma/\pi c}$ and $F_{2A} = \frac{K_{II}}{\sigma/\pi c}$. The results in Table 5.2 are accurate to within 2 % as compared to the exact values of Kitagawa [27].

Table 5.2 Stress intensity factors at tip A of a kinked crack $(\alpha_1 = 45^{\circ})$.

b ₁ /(2a)	F _{1A} [27]	F _{1A} [CRACK]	F _{2A} [27]	F _{2A} [CRACK]
0.01	1.000	0.986	0.003	0.002
0.10	0.998	0.976	0.019	0.018

The stress intensity factors at the crack tip B, F_{1B} and F_{2B} , normalized in the same manner, are shown in Figures 5.9 and 5.10. The results for uniaxial normal stress load are compared with those of Kitagawa, Yuuki and Ohira [27]. These results show that the numerical solution is accurate to within 2 % for all kink angles considered.

Figures 5.9 and 5.10 show that, with an increase in the kink angle, α_1 , the F_{1B} value decreases and the absolute value of F_{2B} increases. Also Figures 5.9 and 5.10 show that the values of F_{1B} and F_{2B} become almost constant as the value of F_{1A} increases.

The problem of a main crack under a biaxial stress aligned with the line of the crack has been chosen to illustrate the accuracy of the numerical solution for a crack with a finite kink. The stress intensity factors for a kink of lengh b_1 - 2a/10 are compared in Figure 5.11 with the results presented by Kitagawa and Yuuki [26] (those results agree with [24,25]). The agreement is good.

(b) Anti-symmetric kinked crack

Let us consider a crack model with two branches as shown in Figure 5.8, i.e. an "anti-symmetric kinked crack".

The stress intensity factors F_1 and F_2 of the anti-symmetric kinked crack are plotted in Figure 5.12 as a function of α_1 for different lengths b_1 . These are normalized by the stress intensity factors for a straight crack with the crack length 2a. It is seen from

Figure 5.12 that unlike in the case of the symmetrically kinked crack, ${\bf F}_2$ never changes sign.

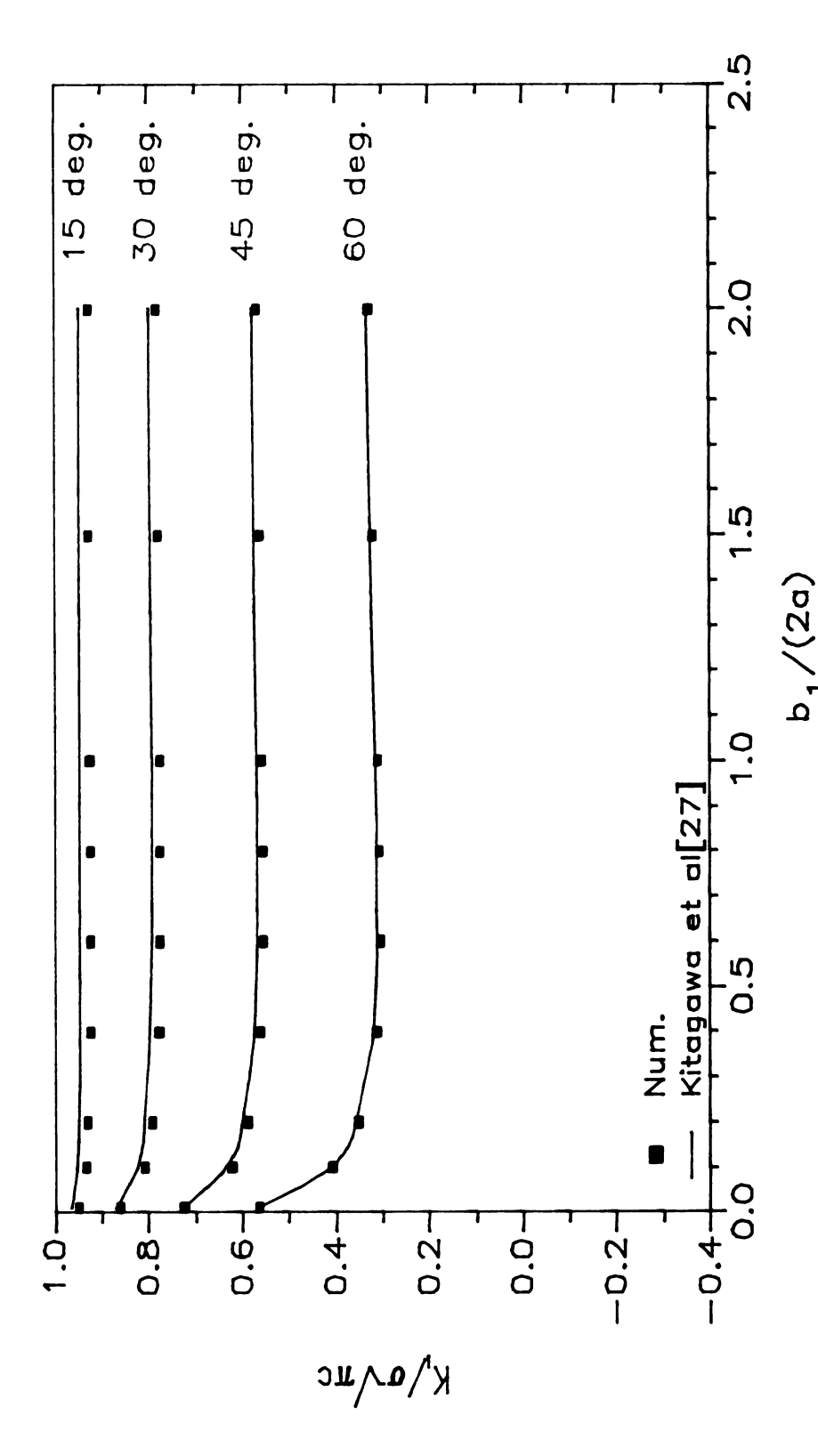
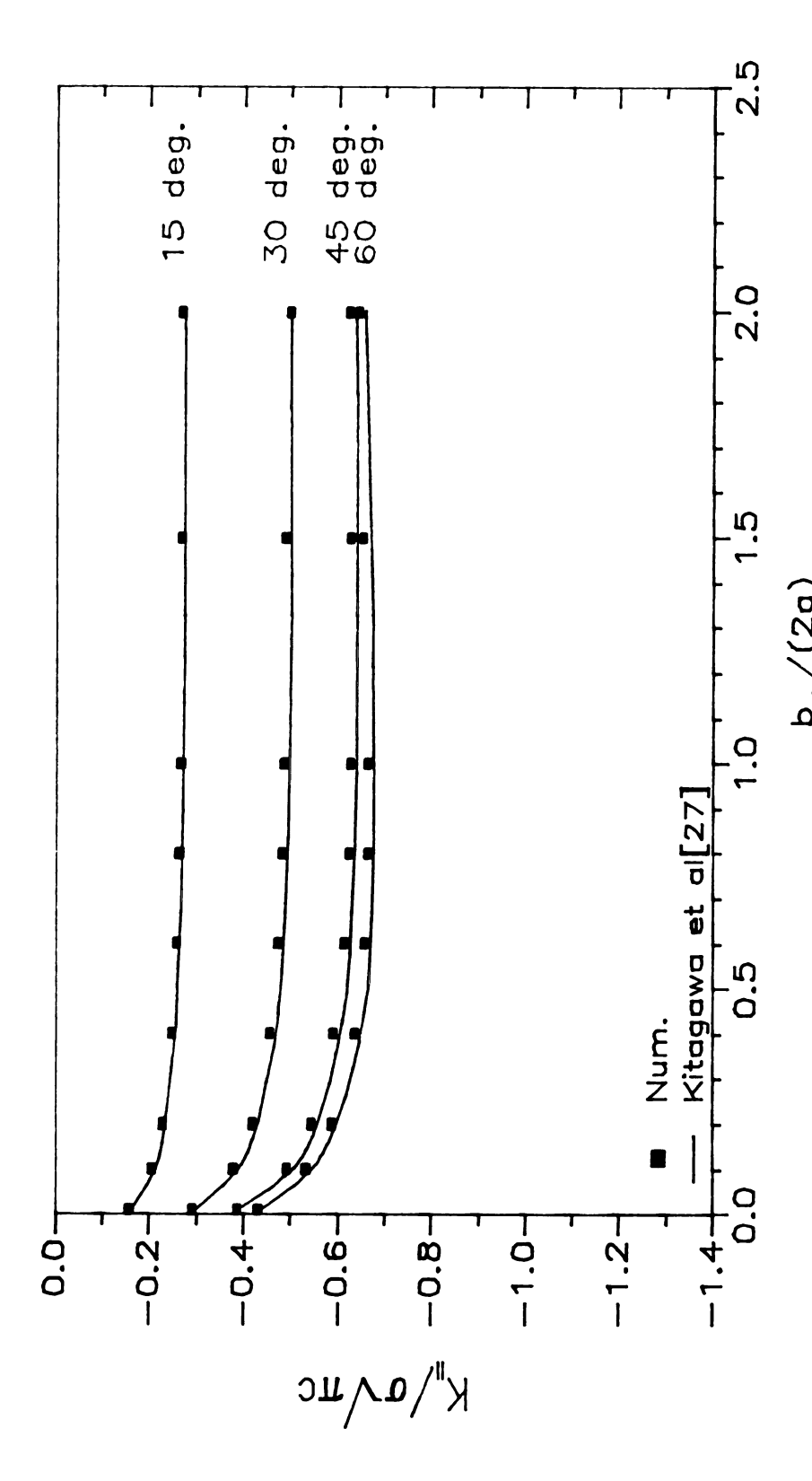


Figure 5.9 Mode I SIFs for an asymmetric kinked crack under uniaxial stress.



Mode II SIFs for an asymmetric kinked crack under uniaxial stress. Figure 5.10

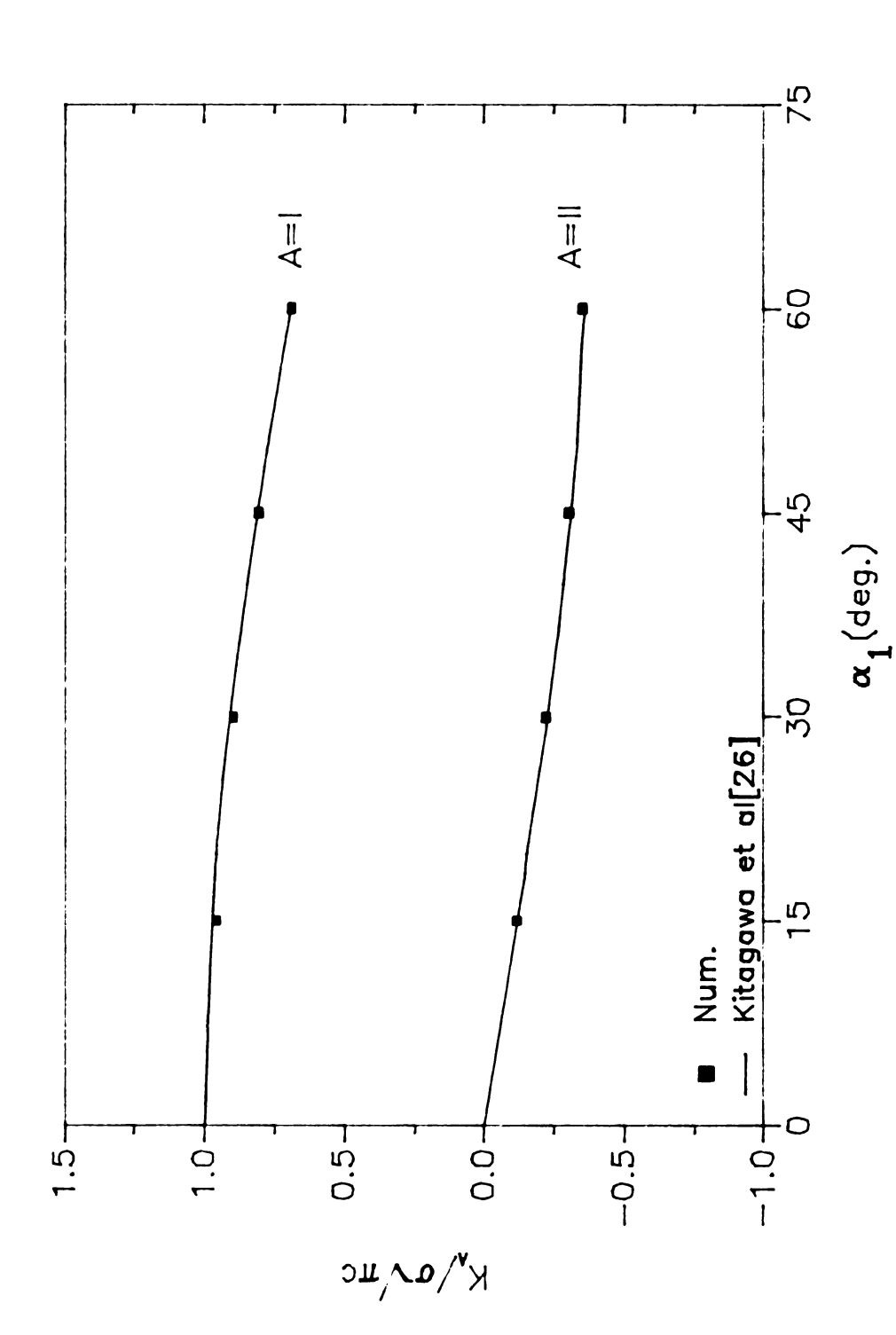


Figure 5.11 SIFs for kinked crack subjected to various biaxial conditions.

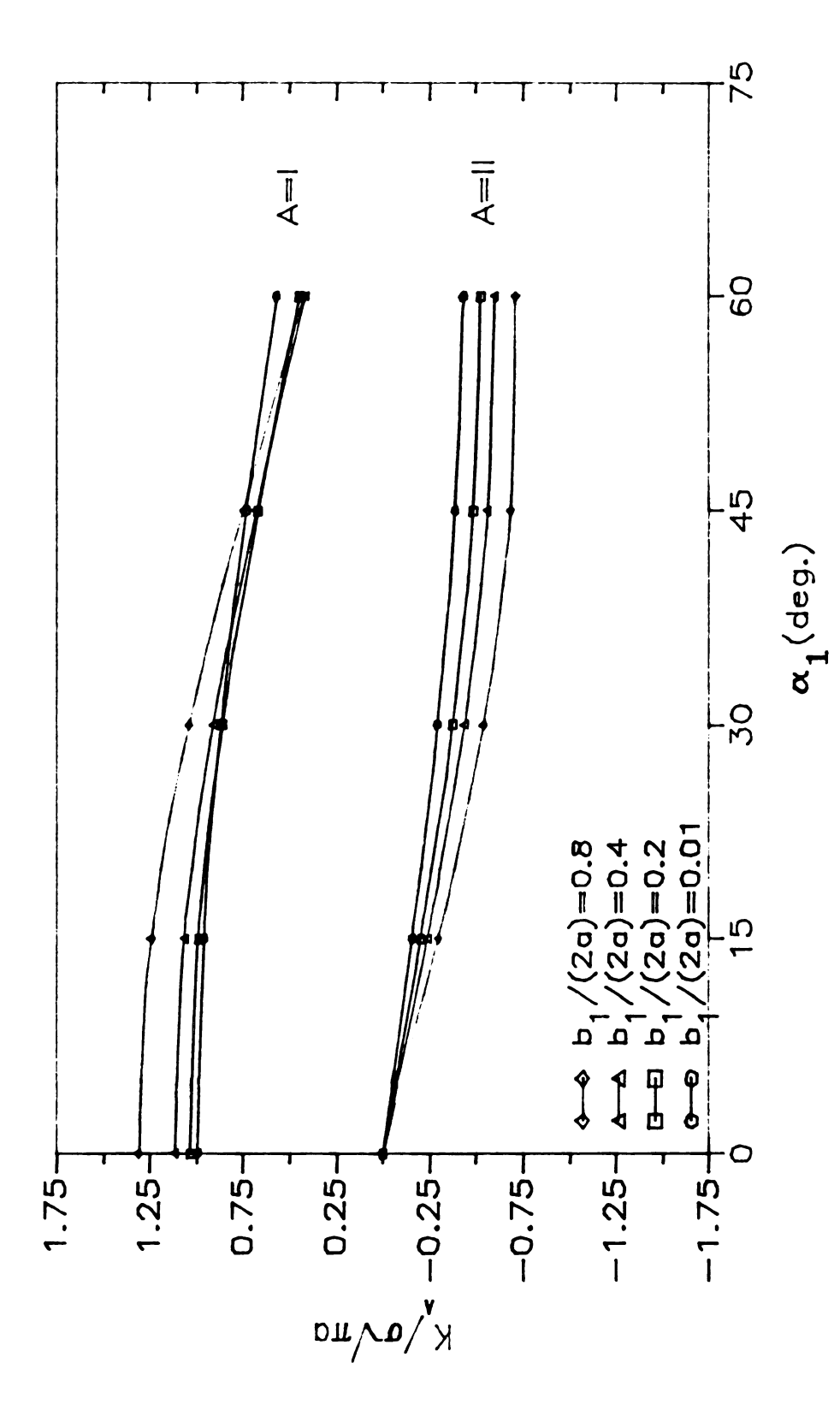


Figure 5.12 SIFs of an anti—symmetric kinked crack in an infinite plate.

5.2 Examples of Finite Domain Problems

Here we employ the coupled model developed in chapter 4 to find numerical solutions for some finite domain problems.

5.2.1 Straight crack

(a) Central symmetric crack with tensile load (Mode I)

The results for the stress intensity factors (SIFs) of the crack problem shown in Figure 5.13 are plotted in Figure 5.14. The length of the crack is varied, while the boundary element mesh is maintained and the same number nodes are used define the crack. With this coupled model, it can be seen that good agreement with the analytical solution of Isida [32] is obtained up to a ratio of a/b = 0.7. For a/b > 0.7, the SIFa are slightly lower than the analytical values.

(b) Central unsymmetric crack with tensile load

The SIFs for the problem shown in Figure 5.15 are given in Table 5.3. Results agree well with the analytical solution given by Isida [32].

(c) Angled crack in a large plate

The results for an angled crack as shown in Figure 5.16 are shown in Table 5.4. Several angles of inclination are considered. As expected, the results are very close to the analytical solution for an

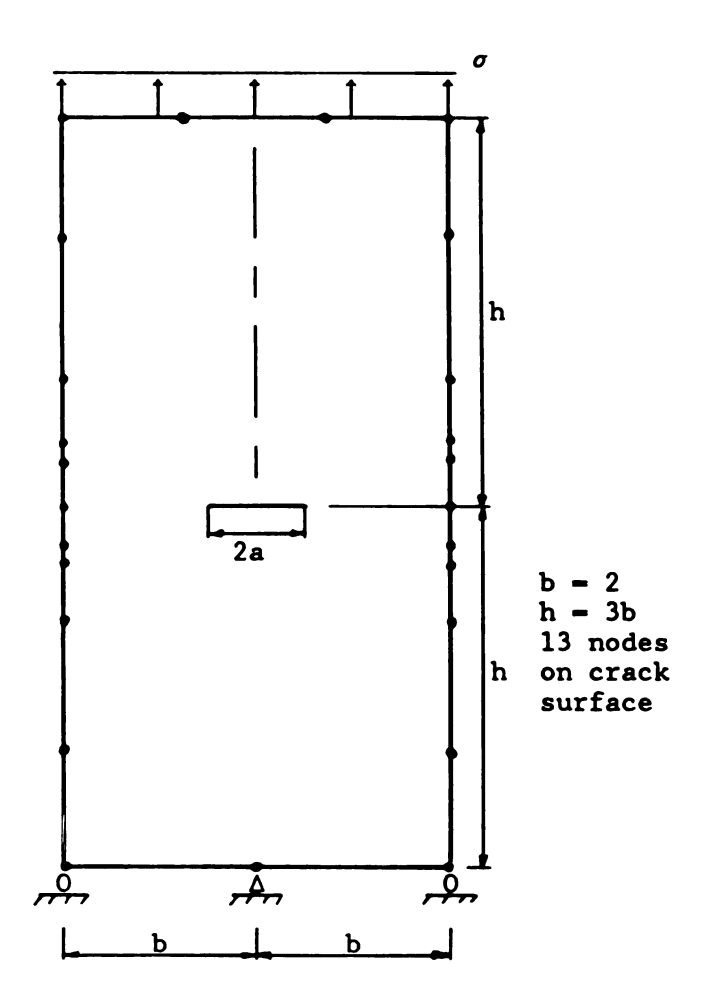


Figure 5.13 Center-cracked test specimen.

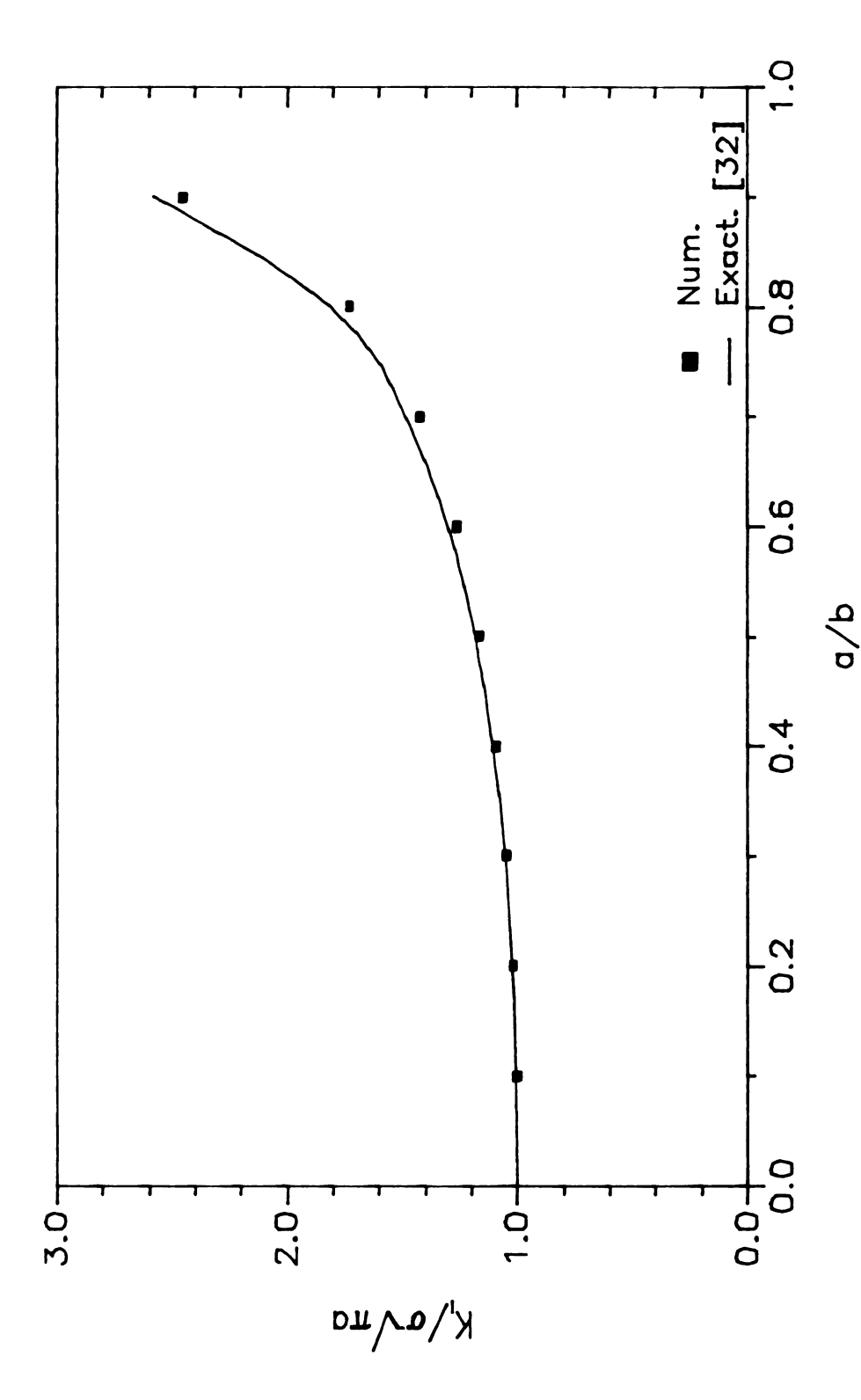


Figure 5.14 SIFs vs. a/b for center—cracked test specimen.

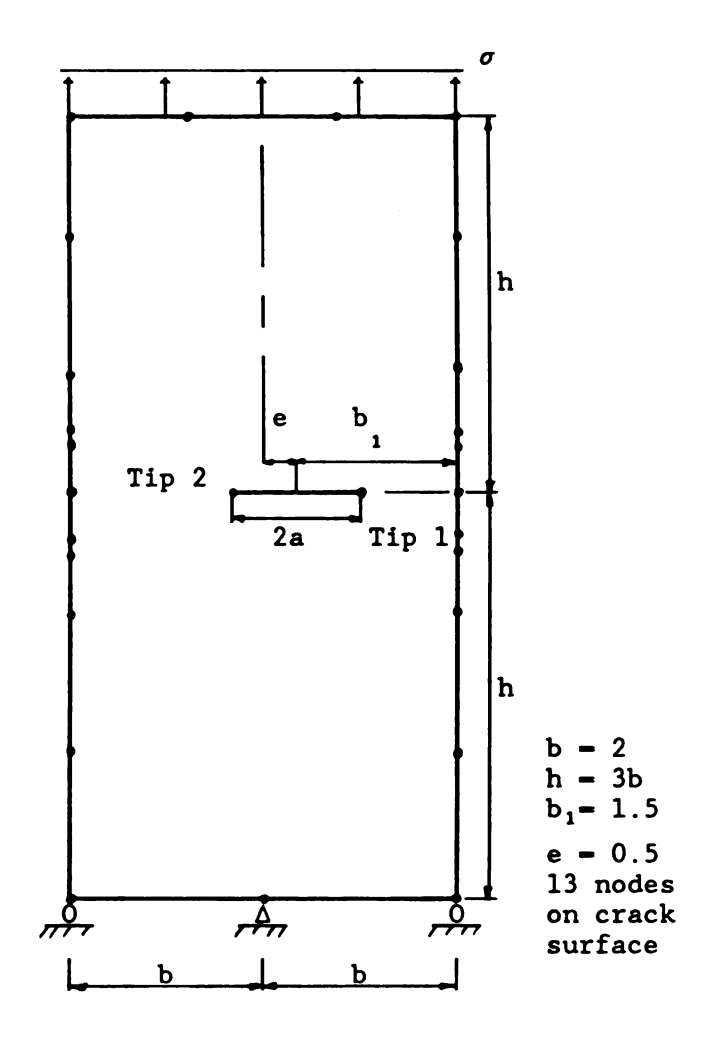
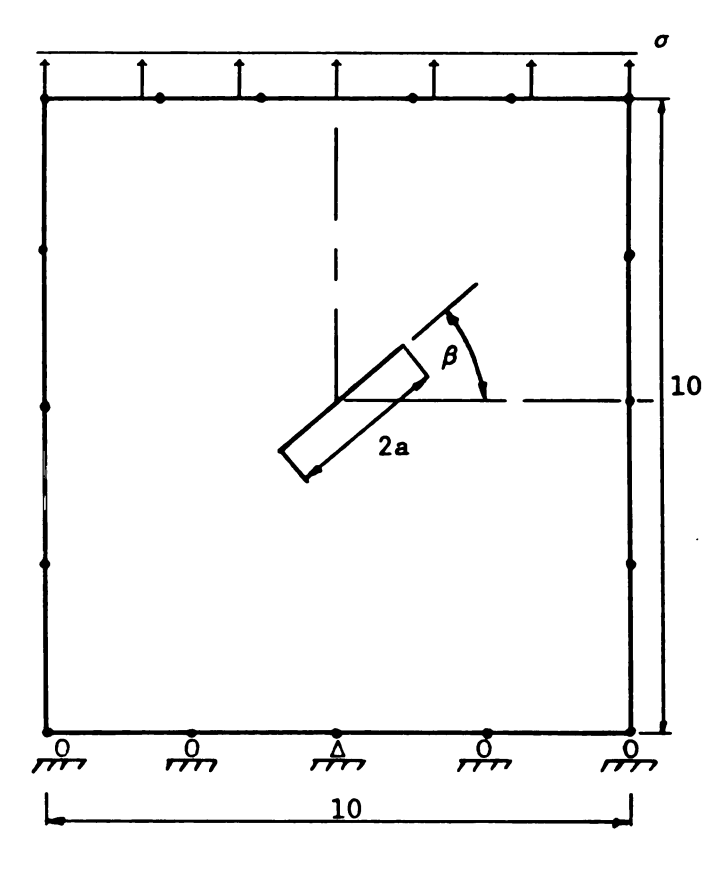


Figure 5.15 An off-center straight crack.



13 nodes on crack surface $2a = \sqrt{2}$ $K_{I} = \sigma/\pi a \sin^{2}\beta$ $K_{II} = \sigma/\pi a \sin\beta \cdot \cos\beta$

Figure 5.16 Angled crack in a large plate.

Table 5.3 Stress intensity factors for an off-center straight crack.

	$\frac{K_{\underline{I}}}{\sigma/\pi a}$ [COUPL]	$\frac{K_{I}}{\sigma/\pi a} [32]$	K _I [COUPL]
Tip 1	1.395	1.405	0.99
Tip 2	1.189	1.200	0.98

Table 5.4. Stress intensity factors for an angled crack in a large plate.

angle(β)	$\frac{K_{I}}{\sigma/\pi a}$ [COUPL]	$\frac{K_{II}}{\sigma/\pi a}$ [COUPL]	$\frac{K_{I}}{\sigma \sqrt{\pi a}}$	<u>K_{II}</u> + σ√πα
90	0.000	0.000	0.000	0.000
60	0.249	0.427	0.250	0.433
45	0.497	0.493	0.500	0.500
30	0.745	0.427	0.750	0.433
0	0.994	0.000	1.000	0.000

+ Analytical solution for an angled crack in an isotropic infinite medium is given by

$$K_{I} - \sigma/\pi a \sin^2 \beta$$
 and $K_{II} - \sigma/\pi a \sin \beta \cos \beta$.

crack in an infinite medium, since the plate is very large compared with the size of the crack.

(d) Angled crack in a plate

Results for the problem shown in Figure 5.17 are given in Table 5.5. Excellent accuracy has been obtained for 45 and 90 cracks, for which analytical results are available.

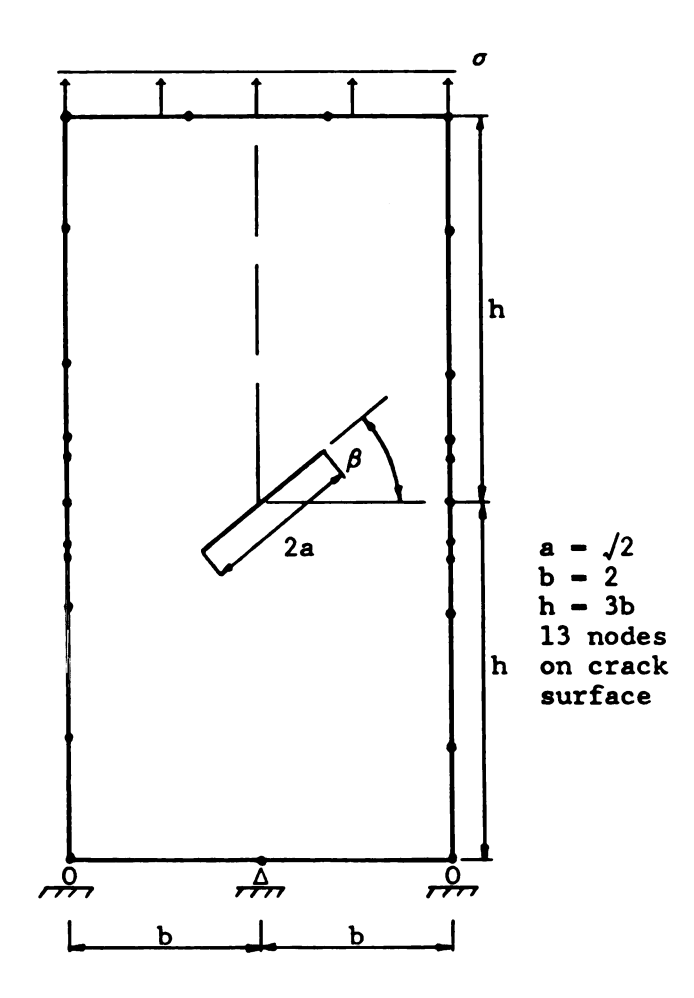


Figure 5.17 Angled crack in a finite plate.

Table 5.5. Stress intensity factors for an angled crack in a finite plate.

angle(β)	$\frac{K_{I}}{\sigma / \pi a}$ [COUPL]	$\frac{K_{II}}{\sigma/\pi a}$ [COUPL]	$\frac{K_{I}}{\sigma/\pi a}$ [32]	$\frac{K_{II}}{\sigma/\pi a}$ [32]	K _I [COUP	r] KII
60	0.363	0.507	-	-	-	-
45	0.713	0.570	0.730	0.600	. 98	. 95
30	1.000	0.467	-	_	_	_
0	1.449	0.000	1.488	0.000	.97	_
3	2. 447	2.000	2.400	1.000	•••	-

5.2.2 Kinked Crack

Because an exact solution does not exist, the kinked crack within a finite body can not provide a simple check on the accuracy of the numerical solution. Nevertheless, let us introduce some of numerical results. Figure 5.20 presents results for an asymmetric kinked crack in a finite body as shown in Figure 5.18 while Figure 5.21 presents results for an anti-symmetric kinked crack as shown in figure 5.19. The tendencies of the numerical results are very similar to those of such cracks in infinite bodies, but have higher values.

Computer CPU times for the problems that have been presented here were less than 10 sec for all cases using the Prime 750 computer.

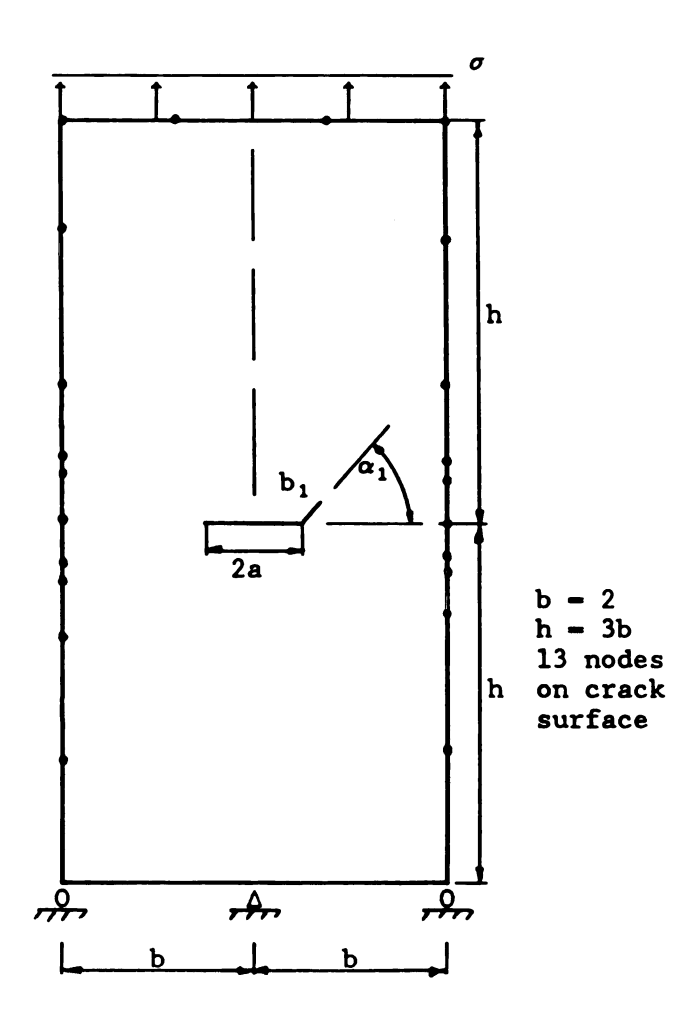


Figure 5.18 Asymmetric kinked crack in a finite plate.

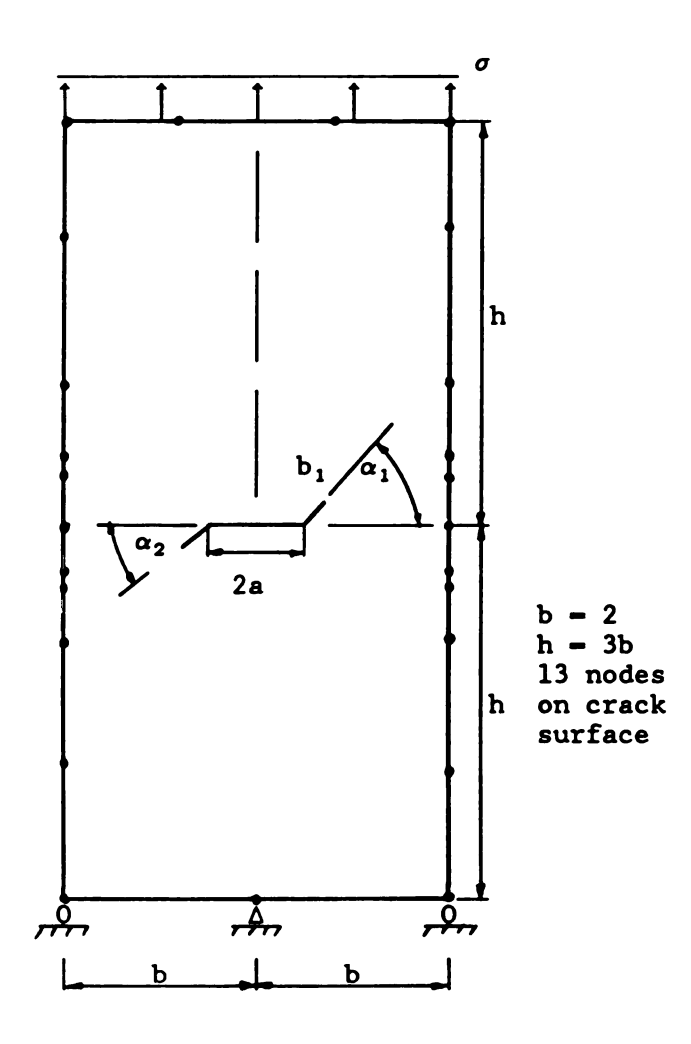


Figure 5.19 Anti-symmetric kinked crack in a finite plate.

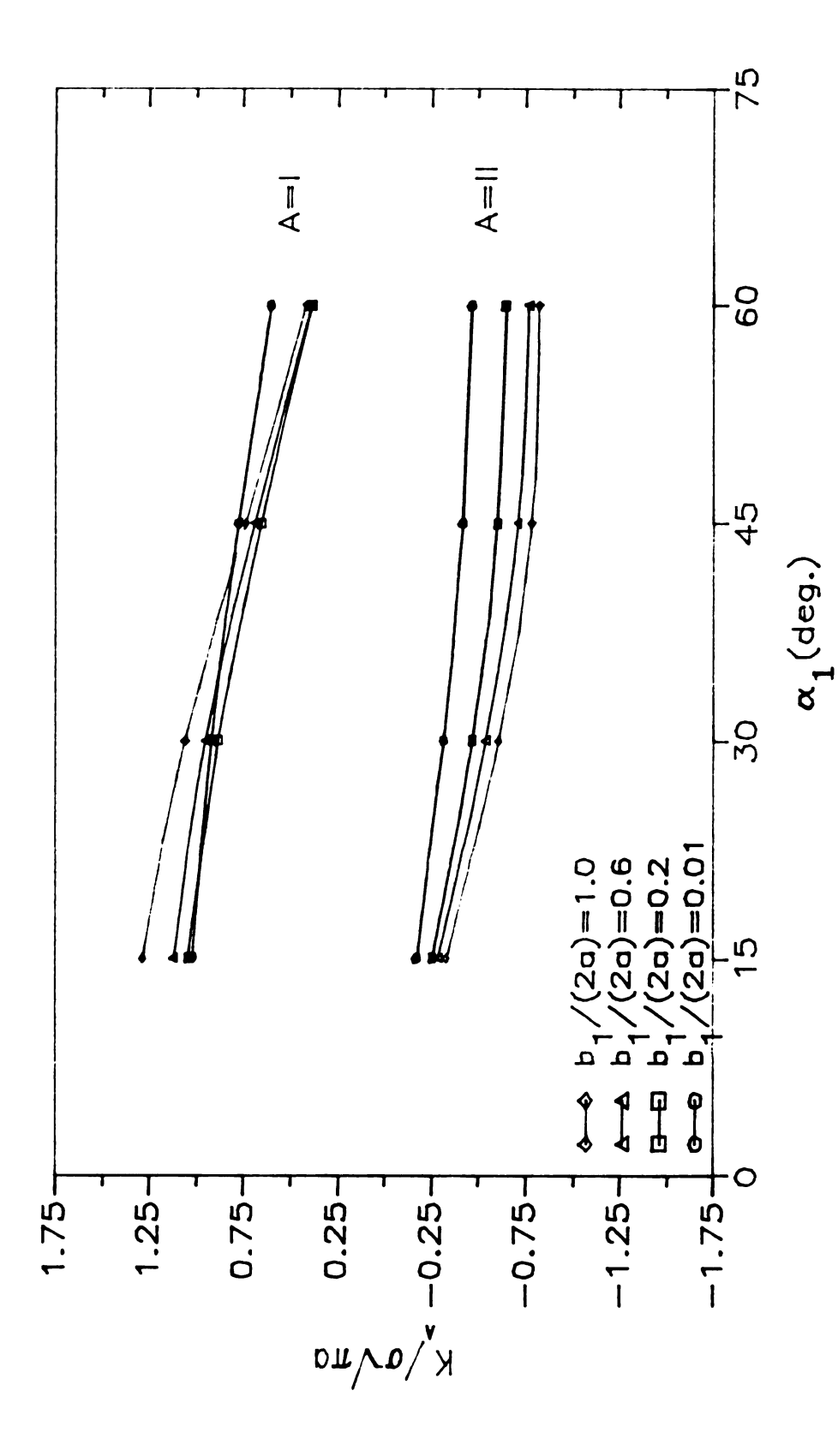


Figure 5.20 SIFs of an asymmetric kinked crack in a finite plate.

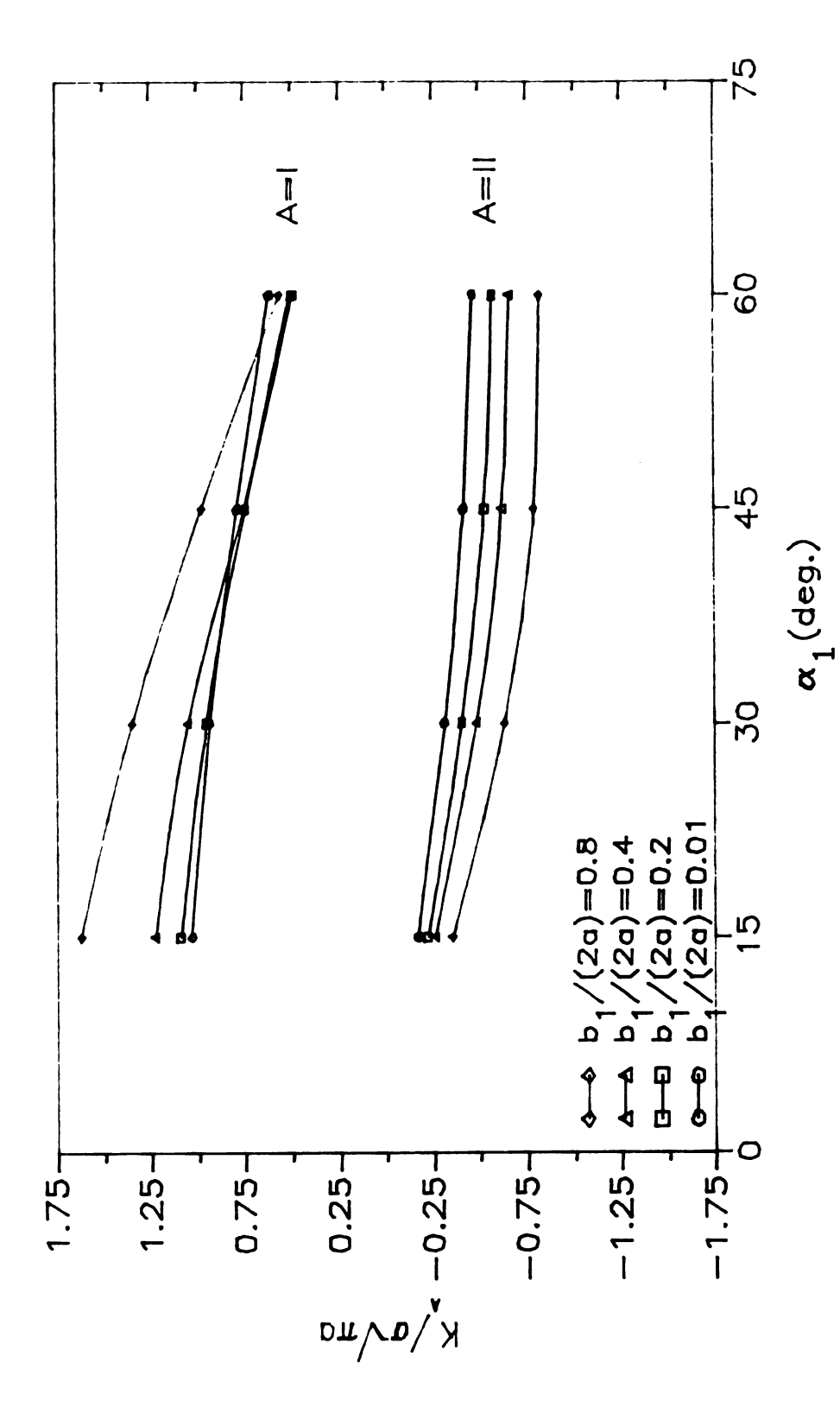


Figure 5.21 SIFs of an anti—symmetric kinked crack in a finite plate.

CHAPTER 6

CONCLUSIONS AND RECOMMENDATIONS

A hybrid method has been presented for the analysis of cracks of arbitrary shape in finite two-dimensional regions. The method has been applied to a number of problems and in all cases, demonstrated accuracy to within 2%. The main advantage of this approach over other techniques is its ability to handle cracks with kinks. Furthermore, only the external boundary and crack needed to be discretized. Thus, analysis of crack propagation problems would require only the addition of nodes to the crack.

In all problems, equal subdivisions were used for numerical treatment. Additionally quarter-point nodes were employed near crack tips. When unequal subdivisions were used, results were not good. This is a limitation of the technique which requires future attention. It is not known at this time why unequal subdivisions do not perform well as such numerical treatment is not precluded by the formulation.

The main advantage of this work is its potential for modelling crack propagation. Unlike the finite element and boundary element techniques, this technique does not require complete re-meshing at each crack growth increment. Rather, it simply requires the addition of meshes along the propagation path.

Three-dimensional crack analysis has not developed as fully as its two-dimensional counterpart because of greater complexities. Consequently, very few exact analysis have been obtained. There are a number of approximate solutions, commonly dependent on exact results to some extent. It is felt that the method presented here could be extended to three-dimensions without unresonable difficulty. What is required are analogous "fundamental" solutions for the three-dimensional infinite domain (Such solutions are available in the literature) and a method for handling the integrated traction terms.

BIBLIOGRAPHY

- 1. T.A. Cruse, Numerical evaluation of elastic stress intensity factors by the boundary-integral equation method, The surface crack: physical and computational solutions (ed. J.L. Swedlow), ASME, 153-173 (1972).
- T.A. Cruse, Boundary-integral equation fracture mechanics analysis, Boundary-Integral Equation Method: Computational Applications in Applied Mechanics (eds. T.A. Cruse and F.J. Rizzo), ASME, AMD-Vol. 11, 31-48 (1975).
- 3. T.A. Cruse, Two-dimensional BIE fracture mechanics, Appl. Math. Modelling 2, 287-293 (1978).
- 4. T.A. Cruse and R.B. Wilson, Advanced applications of boundary-integral equation methods, Nucl. Engr. Design 46, 223-234 (1978).
- 5. M.D, Snyder and T.A. Cruse, Boundary-integral equation analysis of anisotropic plates, Intl. J. Fracture 11, 315-328 (1975).
- 6. T.A. Cruse, Two and three-dimensional problems of fracture mechanics, Developments in Boundary Element Methods 1 (ed. by P.K. Banerjee and R. Butterfield), Applied Science Publishers 97-119 (1979).
- 7. V. Sladek, and J. Sladek, Three-dimensional crack analysis for anisotropic body, Appl. Math. Modelling 6, 374-389 (1982).
- 8. V. Sladek, and J. Sladek, Three-dimensional curved crack in an elastic body, Intl. J. Sol. Struct. 19, 425-436 (1983).
- 9. B.A. Bilby, and J.D. Eshelby, Dislocations and the theory of fracture, in Fracture: An Advanced Treatise Vol. 1 (ed. by H. Liebowitz), Academic Press, 99-182 (1968).
- 10. G.C. Sih, Stress distribution near internal crack tips for longitudinal shear problems, J. Appl. Mech. 24, 51-58 (1965).
- 11. T. Nakayama, Trans. JSME 39 (322), 1779 (1973).
- 12. E. Smith, Crack bifurcation in brittle solids, J. Mech. Phys. Solids 16, 329-336 (1968).
- 13. Y. Yamamototo and N. Tokuda, Lecture at No. 1 Comm. Weld., Jap. Soc. Navalarchitecture (25 oct. 1972): and Doctor Thesis of N. Dokuda, Tokyo Univ., 91 (1974).
- 14. H. Anderson, Stress-intensity factors at the tips of a starshaped contour in an infinite tensile sheet, J. Mech. Phys. Solids 17, 405-407 (1969).

- 15. H. Anderson, Erratum, J. Mech. Phys. solids 18, 437 (1970).
- 16. K. Palaniswammy and W. G. Knauss, Propagation of a crack under general, in-plane tension, Int. J. Frac. Mech. 8, 114-117 (1972)
- 17. H. Kitagawa and R. Yuuki, Trans. JSME, 41 (346), 1641 (1975).
- 18. O. L. Bowie, Methods of analysis and solutions of crack problems (edited by G. C. Sih), P.1, Noordhoff, Leiden, 1973.
- 19. M. C. Hussain, S. L. Pu and J. Underwood, Stain energy release rate for crack under combined mode I and mode II, Fracture Anaysis, Proceedings of the 1973 National Symposum on Fracture Mechanics, Part II, ASTM Special Technical Publication 560, 2-28 (1973).
- 20. K. Palaniswamy and W. G. Knauss, On the problem of crack extension in brittle solids under general loading, Mechanics Today, S. Nemat-Nasser, Editor, Vol 4. Pergamon Press, 87-148 (1978).
- 21. B. A. Bilby and G. E. Cardew, A crack with a kinked tip, Intl. J. Fracture 11, 708-812 (1975).
- 22. B. A. Bilby and G. E. Cardew and I. C. Howard, Stress intensity factors at the tip of kinked forked cracks, fracture 1977, Vol. 3, Univ. of Waterloo Press, 197 (1977).
- 23. V. V. Pudukelanko and N. B. Romalis, Direction of crack growth under plane stress state conditions, Izv. An SSR, MTT 8, 129-36 (1973).
- 24. K. K. Lo, Analysis of branched cracks, J. Appl. Mech. <u>45</u>, 797-802 (1978).
- 25. S. N. Chatterjee, The stress field in the neighborhood of branched crack in an infinite elastic sheet, Intl. J. Sol. Struct. 11, 521-38 (1975).
- 26. H. Kitagawa and R. Yuuki, Analysis of branched cracks under biaxial stresses, Fracture 1977, Vol. 3, Univ. of Waterloo Press 201 (1977).
- 27. H. Kitagawa, R. Yuuki and T. Ohira, Crack-morphological aspects in fracture mechanics, Engineering fracture Mechanics 7, 515-529 (1975).
- 28. V. Vitek, Plane strain stress intensity factors for branched cracks, Int. J. Fracture 13, 481-501 (1977).
- 29. Crouch, S. L., Solution of plane elasticity problems by the displacement discontinuty method, Intl. J. Num. Method Engng. 10 301-343 (1976).
- 30. G. C. Sih, P. C. Paris, and F. Erdogan, Crack-tip, stress intensity factors for plane extension and plate bending problems, J. Appl. Mech. 29, 306(1962).

- 31. N. I. Muskhelishvili, Some basic problems on the mathematical theory of elasticity, Noordhoff, 1952
- 32. H. Tada, P. C. Paris, and G. R. Irwin, The stress analysis handbook, Del Research Corporation, Hellertown, Penn., 1973
- 33. N. Altiero, Integral equation methods in fracture mechanics, Engineering Mechanics in Civil Engineering 1, 132-135 (1984).
- 34. Solveig Melin, On sigular integral equation for kinked cracks Intl. J. Fracture 30, 57-65 (1986).
- 35. Kare Hellan, Introduction to fracture mechanics, McGraw-Hill 1984.
- 36. S. D. Conte and Carl deBoor, Elementary numerical analysis: Algorithmic approach, 3rd ed., McGraw-Hill, N. Y., 1980.